Journal Pre-proof

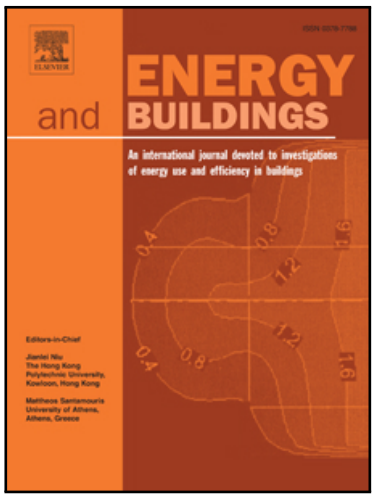

Reducing urban heat stress through green roofs: a modeling-based performance analysis across green roof types and urban morphologies

Thaïs Keravec-Balbot, Mitali Yeshwant Joshi, Srinidhi Gadde, Auline Rodler, Marjorie Musy, Rémy Claverie, Jacques Teller

PII: S0378-7788(26)00388-9
DOI: https://doi.org/10.1016/j.enbuild.2026.117328
Reference: ENB 117328

To appear in: *Energy & Buildings*

Received date: 29 September 2025
Revised date: 12 March 2026
Accepted date: 13 March 2026

Please cite this article as: Thaïs Keravec-Balbot, Mitali Yeshwant Joshi, Srinidhi Gadde, Auline Rodler, Marjorie Musy, Rémy Claverie, Jacques Teller, Reducing urban heat stress through green roofs: a modeling-based performance analysis across green roof types and urban morphologies, *Energy & Buildings* (2025), doi: https://doi.org/10.1016/j.enbuild.2026.117328

Reducing urban heat stress through green roofs: a modeling-based performance analysis across green roof types and urban morphologies

Thaïs Keravec-Balbot[a], Mitali Yeshwant Joshi[b], Srinidhi Gadde[c], Auline Rodler[d], Marjorie Musy[d], Rémy Claverie[e], Jacques Teller[a]

[a]*University of Liège, Urban & Environmental Engineering Department, LEMA Research Group, Allée de la Découverte 9, B52, Sart-Tilman, Liège, 4000, Belgium*
[b]*Copernicus Institute of Sustainable Development, Utrecht University, Princetonlaan 8a, Utrecht, 3584 CB, The Netherlands*
[c]*Water Resources Department, Faculty ITC, University of Twente, P.O. Box 217, Enschede, 7500 AE, The Netherlands*
[d]*CEREMA Equipe BPE, Nantes, F-44000, France*
[e]*CEREMA Est, TEAM Research Group, Tomblaine, 71 rue de la grande haie, F-54510, France*

Abstract

Rising temperatures driven by climate change and rapid urbanization have heightened the need for effective urban cooling strategies. Green roofs, as nature-based solutions, can offer a practical alternative contribution in dense urban areas by improving thermal comfort. However, accurately modeling their microclimatic impact remains difficult due to a large variety in green roof design parameters and limited validation of available tools. In addition, few green roof modeling studies account for urban morphology at the block scale. This study addresses these gaps by validating the green roof module of the Solene-microclimat urban microclimate model with a comparison against measurements and by conducting a local sensitivity analysis of the green roof parameters. The green roof model outcomes were compared to measurements and found to depict physical processes correctly. A local sensitivity analysis investigates how substrate and vegetation parameters as well as irrigation factors affect pedestrian level thermal comfort across nine representative urban morphological archetypes in Liège, Belgium, during a hot summer day. Results show that while irrigation and vegetation characteristics influence outdoor thermal comfort, substrate properties have minimal impact. Well-irrigated, tall, and dense green roofs were found to reduce average pedestrian air temperature by up to 1.4 $^{\circ}C$, compared to average scenario green roof. Additionally, green roofs are most effective in improving pedestrian comfort when green roofs are clustered and located near walkable pedestrian areas. The compact mid-rise + low-rise archetype is found to maximize the benefits of green roofs.

Keywords:

Green roof modeling, Urban microclimate, Thermal comfort, Sensitivity analysis

1. Introduction

In recent years, cities are experiencing a severe rise in temperatures due to a combination of unprecedented urbanisation and global climate change [1]. This is intensifying the urban heat island (UHI) effect, where the urban temperatures are higher compared to the rural counterparts [2]. Frequent extreme heat events such as heatwaves are intensifying the UHI effect increasing human-health risks [3]. Urban green infrastructure like green roofs is a suitable nature-based solution for urban areas as they can be seamlessly integrated into existing buildings especially where space for trees and parks is limited. Moreover, they offer multiple benefits, including strong building cooling potential [4, 5, 6] and improvement of outdoor thermal comfort [7, 8, 9]. Given these multiple advantages, it is important to study green roofs with accuracy and detail.

Green roof studies can be mainly classified based on their investigated benefit: microclimate regulation or thermal comfort improvement [10, 11] or reduction of building energy consumption [12]. Whatever the scale and objective, assessing these benefits at the project stage requires models that accurately represent green roofs. Vera et al. (2018) [13] performed a review of heat and mass transfer in green roof models used in building energy and urban environment simulation tools. They found that very few green roof models are used in urban-scale research [14, 15, 16, 17] and the majority of the examined models concentrate on building energy analysis for energy consumption reduction [13, 18, 19, 20].

Solene-microclimat is a microclimate model dedicated to modeling urban microclimate and building thermal behavior for the assessment of indoor and outdoor comfort. It relies on a three-dimensional tetrahedral mesh with a spatial resolution down to 1 m, allowing an accurate representation of complex urban morphologies and making it a reliable tool for assessing adaptation strategies at the district scale [21]. Its 3D capabilities are based on integrating radiative, thermal, and computational fluid dynamics (CFD) models [21]. Solene-microclimat has been used in multiple studies for investigating different nature-based solutions like trees, lawns, green walls and green roofs [22, 23, 24, 25]. Although different modules of Solene-microclimat have been validated against experimental measurements, including the green wall module [22], the green roof model has not yet been validated [25], which is necessary to conduct further research.

Recently, Joshi et al. (2024) [25] used Solene-microclimat to study the impact of green roofs on microclimate across different urban morphological block archetypes in Liège, Belgium. Their results highlighted that green roofs can reduce surface and air temperature in large low-rise archetypes. However, the study focused on extensive green roofs with fixed properties, without addressing the sensitivity of results to vari-

ations in parameters such as LAI, foliage height, substrate water content, and albedo, which have been shown to strongly influence green roof performance [11, 26]. Since the Solene-microclimat green roof model relies on input parameters related to substrate and foliage properties which are often uncertain or unknown, sensitivity analysis offers a systematic way to evaluate how variations in these inputs affect outdoor microclimate regulation. Previous applications of the model [24, 25] analyzed green roof impacts, but the influence of parameter uncertainty across different urban morphologies remains unexplored. Sensitivity analysis, defined as the study of how input variations influence model outputs [27], can therefore help identify the most influential design elements, improve model performance, and guide green roof implementation strategies.

The methods for sensitivity analysis can be classified into two categories: local and global approaches. Local approaches (also called one-at-time (OAT) methods), quantify the impact on the model output when one factor is changed and all the others are fixed. They require fewer computations but are less effective for complex systems. Global approaches (also called all-at-a-time (AAT) methods), are related to the influence of uncertain inputs over the whole input space, by considering multiple variables simultaneously. They have been largely used in building thermal simulations but rarely with a large multiplicity of factors [28], and rarely in green roof studies.

Table 1 provides a summary of the sensitivity analyses conducted on green roof models.Both local and global sensitivity analysis studies specifically addressing green roof temperature models are relatively limited. Most of the studies widely apply sensitivity analysis in thermal building simulations focusing on thermal fluxes through the roof or energy consumption. Nevertheless, most of the green roof parameters in Solene-microclimat are also used in other models, and their impact on various results has been explored in Table 1. Few studies [29, 30] have examined a broad range of parameters, and none have accounted for all relevant factors. All studies agree on the important influence of LAI and substrate thickness. While some have conducted rigorous sensitivity and uncertainty analyses, they highlight the need for a systematic evaluation of how green roof performance depends on various parameters.

Moreover, the lack of a comprehensive and accurate database of green roof properties poses a challenge for researchers and practitioners, as it limits the ability to simulate green roofs realistically and may lead to inaccurate estimations of the thermal loads in buildings incorporating such systems [31, 32].

Building on above literature survey, four research gaps are identified:

1. While the Solene-microclimat green roof model has been used, it has not yet been validated against experimental measurements.

2. Existing studies have been conducted with a fixed urban morphology, making their results highly dependent on specific urban contexts. There is no study that investigates the green roof parameters along with urban morphological characteristics for microclimate regulation.

3. There is a significant gap in the literature regarding a rigorous, comprehensive evaluation of green roof parameters from a thermal outdoor environment perspective, as well as a lack of proper assessment of the influence of all parameters and their possible interactions.

4. There is no established database of vegetation and soil parameters for scientists and practitioners to reference when field data is unavailable for green roof models [31, 32]. This lack of reference values introduces uncertainty and hinders reliable simulations.

Sensitivity analysis can offer valuable insights by identifying the most influential parameters, guiding data collection efforts, and optimizing calibration strategies [33]. Therefore, this study aims to address the above research gaps by identifying the green roof parameters that most significantly contribute to mitigating pedestrian outdoor thermal stress during hot days for the urban morphological block archetypes in Liege, Belgium using sensitivity analysis. The analysis starts with the green roof model implemented in Solene-microclimat, identifying the key input parameters and defining their value ranges based on existing literature. An experimental validation of the green roof model is performed to show that the model represents green roof temperatures correctly. A sensitivity analysis is then performed, testing each parameter at three levels (minimum, baseline, and maximum), to evaluate their impact on pedestrian thermal stress reduction across the nine distinct urban block archetypes identified in Liège.

This study aims to address the aforementioned research gaps by identifying the green roof parameters that most strongly contribute to reducing pedestrian outdoor thermal stress during hot days across representative urban block archetypes in Liège, Belgium, using sensitivity analysis. First, the Solene-microclimat green roof model is introduced, and its thirteen key input parameters are identified. Their value ranges are defined based on a review of the existing literature, thereby investigating gap 4. An experimental validation of the green roof model is then conducted to demonstrate its ability to accurately reproduce green roof temperatures, examining gap 1. Subsequently, a local sensitivity analysis is then performed, testing each parameter at three levels (minimum, baseline, and maximum), to evaluate their impact on pedestrian thermal stress reduction across the nine distinct urban block archetypes identified in Liège, thereby addressing gaps 2 and 3.

Reference	Model	Outcome	Parameter	Method	Result
[34]	Energy balance model	TF	Water availability of the soil and convection coefficient	OAT (2 values per parameter)	Convection coefficient and water availability are the factors that regulate heat storage
[35]	Energy balance model	TF	Foliage height, LAI, soil and insulation thickness, roof type, humidity, and wind speed	OAT (3 values per parameter)	The vegetation most important parameter is LAI as it influences transpiration and shading
[36]	Heat/moisture model	TF	Thickness of soil layer and LAI	AAT (18 cases)	Soil thickness drives year-round performance; LAI matters in summer
[37]	Heat/moisture model	TF	Dry thermal conductivity, water content, density, thickness of substrate and drainage layers	OAT and AAT	The dry conductivity and thickness of layers are more influential parameters
[38]	EnergyPlus	BEC	Thickness of soil and plant density	OAT (2 values per parameter)	Thicker soil and denser plants in summer enhance green roof performance
[39]	EnergyPlus	BEC	Irrigation schedules, plant height, substrate type and LAI	OAT and some combinations	LAI most influences the energy use, while plant height has no effect
[40]	EnergyPlus	BEC	The type of substrate, LAI, the roof structure material and the insulation levels	OAT and some combinations	Vegetation reduces cooling loads more than insulation, while insulation impacts heating more
[30]	EnergyPlus	BEC	16 parameters	AAT (4 values per parameter)	The key factors reducing cooling demand are construction R-value, LAI, substrate thickness and conductivity
[41]	EnergyPlus	BEC	Growing media depth, plant canopy density, climate and building use	AAT	In cooling-dominated buildings, LAI has a greater impact
			LAI, plant height, dry soil conductivity	OAT (20 values per parameter)	LAI has the most impact on building thermal gain
[42]	Energy Plus	Building thermal gain	11 parameters	OAT (2 values per parameter)	Only four parameters significantly affected thermal gain: LAI, plant height, dry soil conductivity, and minimum stomatal resistance
[29]	Urban hydrological model	TF and temperatures	15 parameters	AAT (Monte Carlo)	Green roof performance is sensitive to aerodynamic resistance, soil hydraulics, and thermal properties
[43]	Heat/moisture model	Vegetation and indoor temperatures	Incident solar radiation, ambient temperature, evapotranspiration rate, wind speed	AAT (Monte Carlo)	Indoor temperature is most affected by ambient temperature and solar radiation, and least by wind speed
[31]	Envi-met	Pedestrian comfort indices	LAI, leaf angle distribution, substrate emissivity and water coefficient, air gap behind the substrate	OAT (3 values per parameter)	LAI is the most significant parameter. Remark : Green roof and facade models are the same but the study is on green facades
[44]	Energy-Plus	BEC	Stomatal resistance, soil surface roughness, plant height and substrate thickness	OAT	Substrate height and plant height have the most significant impact on energy savings
[45]	Energy-Plus	BEC and TF	Vegetation height, LAI, stomatal resistance, substrate thickness, conductivity, density and heat	OAT (1944 combinations)	In temperate climate, low LAI, high substrate thickness and low thermal transmittance was best

2. Methodology

2.1. Solene-microclimat model

Solene-microclimat is dedicated to modeling urban microclimate and building thermal behavior for the assessment of comfort. It is used to assess climate adaptation measures at the district scale [21]. Its 3D capabilities are based on integrating radiative, thermal, and computational fluid dynamics (CFD) models [21]. Unlike other urban microclimate models, Solene also has the advantage of representing urban blocks faithfully due to tetrahedral meshing with spatial resolution of the model depending on the meshes and up to 1 m. The simulation can be launched for hourly or sub-hourly time steps. Different kinds of nature-based solutions can be considered: trees [46], green areas [47], green roofs and green walls [22, 23, 24] as well as lawn surfaces [48]. The Solene-microclimat green roof model includes numerous parameters. A full description of the physical processes and thermal balances is available in Malys et al. (2014) [23].

2.2. Sensitivity analysis

The objective of this study is to analyse the influence of green roof parameters on the outdoor thermal comfort in summer conditions, using Solene-microclimat. The Solene-microclimat green roof model uses 12 parameters, listed in Sec. 2.3. A one-day simulation for a neighborhood sized mock-up takes several hours to complete on a supercomputer. However, performing a global sensitivity analysis requires lots of runs to investigate the interactions between parameters. Therefore, performing a global sensitivity analysis over 12 parameters was not possible. A local screening approach to identify the most influential variables is performed.This sensitivity analysis can screen dominant first-order parameter effects already and determine which parameters have a significant influence on the effect of green roofs on pedestrian thermal comfort.

In this study, multiple simulations were run for various morphological block archetypes and green roof parameters to analyse the influence of green roof parameters on the outdoor thermal comfort in summer conditions. The simulations were performed on supercomputers for multiple morphological block archetypes in the city of Liége, Belgium [49]. This work uses the block archetypes from Joshi et. al. (2024) [25], described in Section 2.5. In this paper, the authors investigated the impact of green roofs on microclimate in Liége, Belgium, using Solene-microclimat model. They identified 27 July 2018, the hottest day of an intense heatwave, as the reference for their simulations. The same day is adopted for our sensitivity analysis (see [25] for detailed meteorological conditions), simulating the microclimate between 7 AM and 9 PM, focusing on daytime variation.

To assess the impact of green roof parameters on outdoor thermal comfort, the analysis focuses on walkable surfaces (lawns and impervious areas) within urban block archetypes. Given that air temperature alone is insufficient for evaluating comfort, a thermal comfort index is needed. In this study the Rothfusz (1990) [50] equation, commonly used by the American National Oceanic and Atmospheric Administration (NOAA), is adopted to account for the combined effect of temperature and humidity on perceived heat.

The heat index is calculated as the output of the sensitivity analysis, considering 12 green roof parameters across nine urban morphologies. Since this involves a large number of simulations, the code was parallelized and executed on high-performance computing systems: the NIC5 supercomputer (Université de Liège) and the Dutch national supercomputer, Snellius.

For the local sensitivity screening, each parameter is assigned a low, baseline, and high value. Varying one parameter at a time, the selected day (7 AM–9 PM) is simulated across the nine block archetypes. Outputs (air temperature, humidity, and heat index) are computed over the mesh and compared to the baseline simulation to assess the parameter's influence. The workflow is summarized in Fig. 1, with parameter ranges listed in Table 2. In total, 225 simulations are performed.

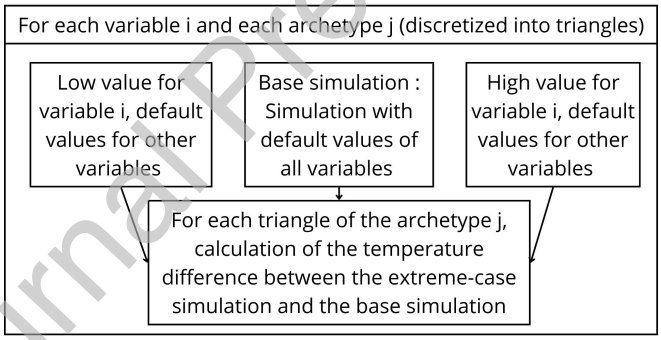

Figure 1: Simulation method: Simulation workflow for the local sensitivity screening. Each variable is tested at its minimum and maximum values while keeping the others at default settings. Results (temperature, humidity, heat index) are compared against the baseline simulation.

2.3. Green roof parameters

2.3.1. Structural parameters

The green roof vegetation in Solene-microclimat is represented by five parameters : Leaf Area Index (LAI), which is the total surface area of leaf compared to the total surface area of ground, foliage height, extinction coefficient used to calculate the transmission of solar radiation through foliage, emissivity, and albedo. For LAI, foliage height, emissivity and albedo, Table 12 in Appendix A presents the ranges of values

used in green roof parametric studies or sensitivity analysis, which serve for selecting the low, default, and high values used in our analysis.

LAI is a key vegetation variable widely studied [51] and measurable through harvesting, light interception [52], or satellite data [53, 54]. Together with foliage height, it is commonly used in green roof models due to data accessibility and their role in energy and mass exchanges [13]. While several studies have shown correlations between LAI and foliage height depending on vegetation type [55, 56, 57], there is no consensus on a universal relationship, particularly in the context of green roofs. As a result, LAI and the foliage height are treated as independent parameters in this study.

The extinction coefficient is used to account for shading in most green roof models [13]. The extinction coefficient is calculated from the leaf angle and solar orientation [58, 59]. Based on extinction coefficient considered in several studies [60, 61, 62, 63, 64], the extinction coefficient is taken between 0.5 and 0.9.

The substrate is described by several parameters : its thickness, conductivity, density and specific heat. There is a strong relationship between substrate conductivity and its mass [65] and material conductivity, density, and capacity are generally interrelated [66]. However, to avoid introducing additional errors, the substrate properties are considered independent. Table 13 in Appendix A highlights the substrate properties taken in green roof studies on which the choice of low, default and high values for the analysis is based.

2.3.2. Process-related parameters

Evapotranspiration is the dominant physical heat transfer process in green roofs. In Solene-microclimat, it is estimated based on the FAO guidelines [57].The model incorporates adjustment coefficients that distinguish soil evaporation and plant transpiration (the foliage transpiration coefficient, α_{lat}, that quantifies the part of transpiration in evapotranspiration) and water disposability (the irrigation coefficient f, that quantifies the magnitude of evapotranspiration) to calculate a suitable evapotranspiration. The derivation of these coefficients and its values are presented in Appendix A.

Another coefficient, the canopy air rate coefficient α_R, is used to calculate the air exchange rate in the canopy according to Eq. 2.3.2:

$$R(v) = R_{min} + (R_{max} - R_{min}) \times \alpha_R \times \frac{v}{v_{max}} \tag{1}$$

R represents the air exchange rate in the canopy, depending on v the wind speed, taken as maximum value $v_{max} = 10m.s^{-1}$. It is usually between 125 and 1000 h^{-1} [58]. Therefore, the maximum and minimum

of the value, R_{min} and R_{max} are taken as $R_{min} = 125\ h^{-1}$ and $R_{max} = 1000\ h^{-1}$. Most generally, α_R is taken equal to 1. α_R is the only one of the considered parameters that isn't related to a real physical parameter but more a calculation parameter. To investigate the impact of the dependency of R to the wind on the green roof performance, the wind speed coefficient will be taken between 0.8 and 1.2.

Table 2 presents the final variation range for the parameters, as well as the low, default and high values.

Parameter	Low	Default	High
Foliage transpiration coefficient α_{lat} [−]	0.5	0.75	1
Irrigation coefficient f [−]	0.1	0.75	1.5
Wind speed coefficient α_R [−]	0.8	1	1.2
Extinction coefficient k_s [−]	0.5	0.7	0.9
Foliage height [m]	0.05	0.25	0.5
LAI [−]	1	2.5	5
Substrate heat capacity [$J.kg^{-1}.K^{-1}$]	700	950	1200
Substrate conductivity [$W.m^{-1}.K^{-1}$]	0.2	0.6	1
Substrate density [$kg.m^{-3}$]	600	950	1300
Substrate thickness [m]	0.1	0.2	0.3
Foliage albedo [−]	0.2	0.3	0.4
Foliage emissivity [−]	0.85	0.9	0.95
Urban morphology	9 block archetypes (A → I)		

Table 2: Final values for the 13 green roof parameters

2.4. Experimental validation of green roof model

Before conducting the sensitivity analysis, the green roof model in Solene-microclimat is validated. Experimental data collected in Nancy, France by the CEREMA (coordinates : 48° 41' 13.457"N, 6° 13'8.444" E) is used. Nancy is a medium-size city, located in the East of France with a Köppen classification Cfb (temperate, no dry season, warm summer), the same as Liège. The set up is presented in Fig. 2a. The isolated green roof is used to perform the validation.

The 5 m^2 studied green roof is composed of (Fig 5 (b)): (1) a vegetation layer, whose composition has been studied by [67] (mostly sedum), (2) a 10 cm substrate layer (pouzzolana, recycled terracotta, terracotta sand, coal slag and compost in unknown proportions), (3) a 5 cm drainage layer (composed of expanded clay beads), (4) a 17.5 cm concrete layer and (5) a 10 cm false ceiling.

This study focuses on the green roof and its surrounding environment, the scale at which observations are available. Consequently, simulations are carried out at a 1 m resolution. To simulate atmospheric conditions to which the green roof is exposed, a series of locally observed meteorological fields are prescribed hourly: atmospheric pressure, shortwave incoming solar radiation (direct and diffuse), longwave incoming radiation, air temperature, relative humidity and average wind speed. These meteorological data

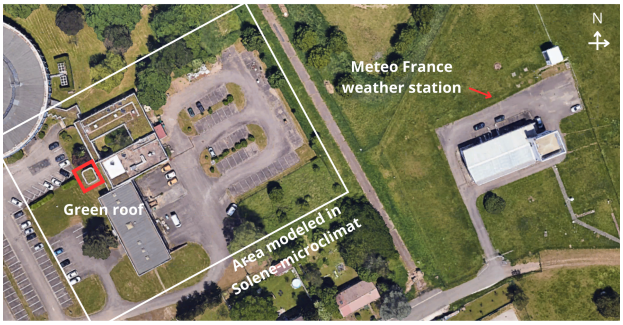

(a) Experimental set-up

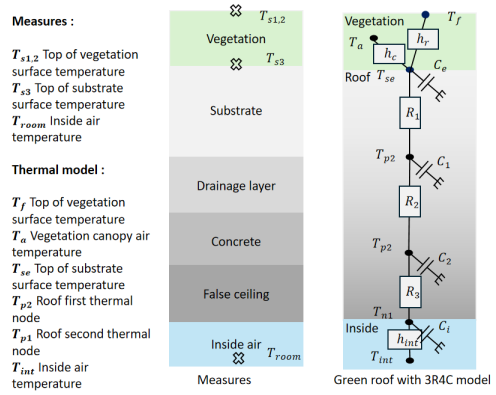

(b) Thermal nodes in Solene-microclimat (right) and experimental measurements (left)

Figure 2: Experimental set-up and thermal model

are obtained from a nearby Meteo France weather station (coordinates : 48° 41' 17.267"N, 6° 13' 16.943" E). The model is assessed under meteorological conditions consistent with those applied during the local sensitivity analysis, therefore for a hot summer day. Comparing the measurements available to the meteorological conditions forced for the 27th July 2018 in Liège, the closest days found are the 19 to 23 June 2023. Meteorological hourly forcing is based on Meteo France weather station data and depicted in Fig. 3.

Based on plans, construction information and Google Maps data, a geometry is created in Solene-microclimat to represent the studied green roof and its surroundings. The whole CEREMA building is represented, with its green roofs, with the surrounding parking lot and urban vegetation.

Typically, Solene-microclimat uses a 3R4C green roof model, inspired by the model of Fraisse (2002) [68], in which two thermal nodes are placed within the building layer to accurately calculate conductive fluxes (see Fig. 2b). Soil temperatures are recorded using PT100 sensors at different depths, including two measuring foliage surface temperature, one measuring the substrate surface temperature and one measuring the inside temperature. This last value is used in Solene-microclimat to set the indoor temperature as a boundary condition.

Based on the literature and construction data, the type of building and the construction year, the wall and roof composition will be taken as displayed in Table 10 in Appendix A. The characteristics of the materials are presented in Table 11 in Appendix A.

The remaining green roof parameters, such as albedo and LAI, need to be defined, and various combinations are explored to identify the most suitable configuration. Multiple simulations were performed and the best one was for a LAI of 2, a foliage height of 0.25 m and an extinction coefficient of 0.9. Hydro-

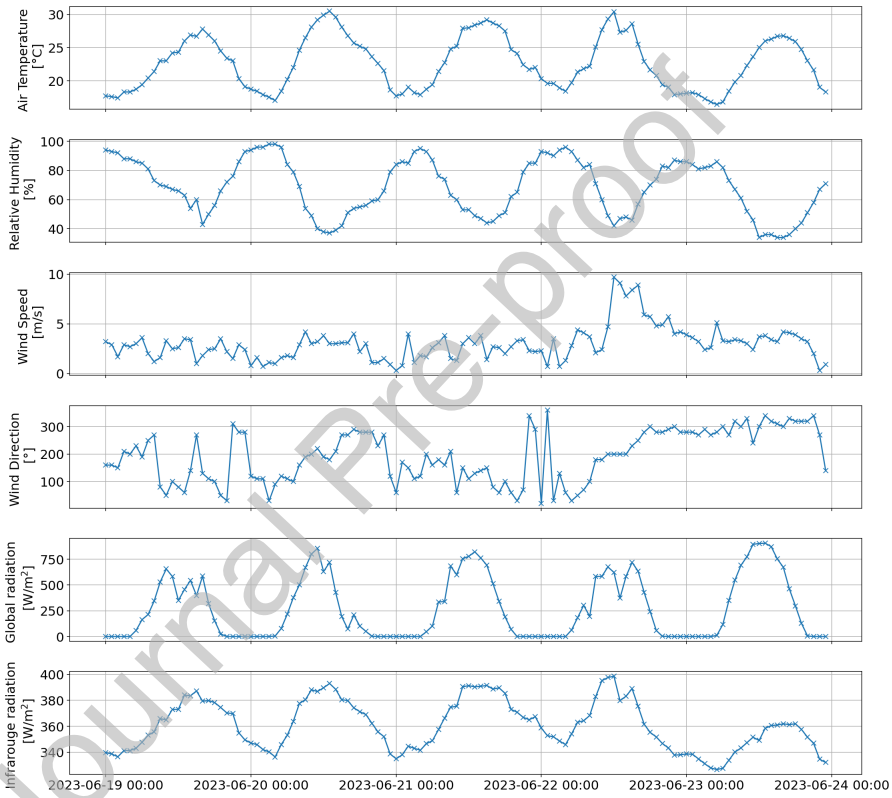

Figure 3: Meteorological conditions used for the experimental validation

logical parameters were derived from substrate moisture measurements and hydrological determination of the substrate, which gives θ_{WP} = 5 $m^3.m^{-3}$ and θ_{FC} = 24 $m^3.m^{-3}$ for the substrate under study. The dry conductivity of the substrate was determined by De Munck et al. [16] and combined with the substrate water content to obtain the substrate conductivity.

The validation focused on comparing simulated and measured green roof 2m air temperature, foliage, and substrate surface temperature.

2.5. Urban block archetypes

This study aims to determine which parameters have the greatest impact on green roof performance with respect to thermal comfort, by systematically evaluating all relevant factors. One parameter that has received limited attention in the literature is the type of building supporting the green roof and the surrounding urban morphology. Urban morphology is defined as a range of spatial and structural characteristics that shape the physical form of urban areas. To account for this, the present study incorporates the urban block classifications developed by Joshi et al. [49] for the city of Liège, using them as a proxy for urban morphology in the sensitivity analysis. This classification identifies nine distinct urban block typologies, derived through a PCA-based k-means clustering applied to 17 urban morphological parameters (Fig. 4).

The spatial resolution is set to 2 meters, as the Solene-microclimat model has been previously validated for urban mitigation strategies at similar grid resolution [69]. At this resolution, running all simulation cases required approximately 500000 core-hours on the Snellius supercomputer of the Netherlands Organization for Scientific Reseach, using 16 cores per case. Tab. 8 and 9 in Appendix A highlight the properties of urban surfaces taken for the modeling. The roofs are composed of a concrete layer, with additional foliage and substrate for the green roofs. For the lawns, properties were taken similarly from previous studies [22, 69] : LAI = 2, k_s = 0.75, f = 1, α_{lat} = 0.75.

The meteorological data, namely air temperature, wind velocity, wind direction, global radiation, direct and diffused radiation, infrared radiation, relative humidity and pressure, are obtained from the observations of the Royal Meteorological Institute, Belgium (RMI).

3. Results

3.1. Experimental validation

A validation was conducted to support the main objective of this study, which is to investigate outdoor thermal stress.

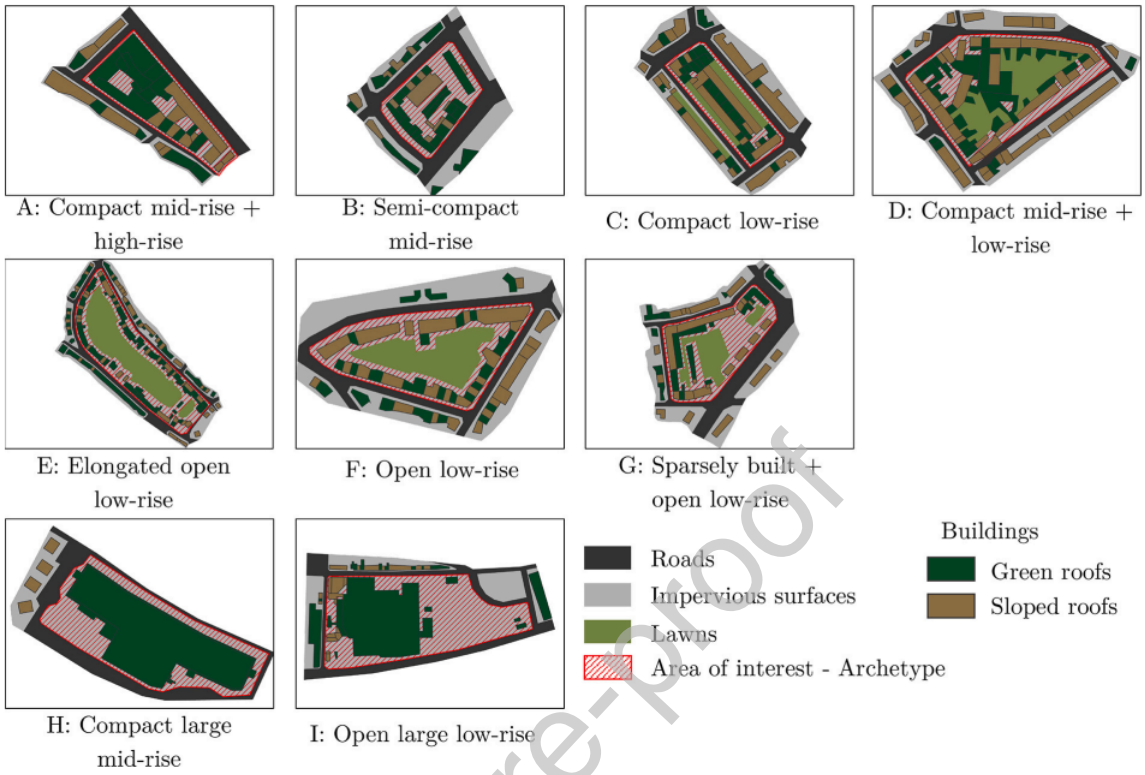

Figure 4: Detailed geometries based on urban morphological block archetypes for the Liege city (from [25])

Fig. 5a and 5b show the comparison of the model outputs and the measurements. The surface temperature results show that the RMSE is 2.70 °C for the substrate temperature and 4.4 °C for the foliage temperature. According to Vera et al. [13]'s review of green roof models, most models are generally more accurate in predicting surface substrate temperature (within 1–3.5 °C) compared to leaf surface temperature (within 1.9–3.9 °C). The results here are consistent with this review, as the substrate temperatures were also better predicted than foliage temperatures.

The main discrepancy in foliage temperature lies in nighttime values, which the model tends to overestimate. For instance, the average minimum model vegetation temperature for the last 3 days is 24.35 °C while for the measurements it is 17.3 °C. The vegetation evening and nighttime cooling is largely underestimated. This could be due to underestimated nighttime convection or long-wave radiation. In contrast, the substrate temperature at night aligns more closely with measurements. Since the analysis will focus on daytime and early evening periods, this limitation is not critical for the following sensitivity analysis.

The validation statistics were calculated over the entire simulation period to maximize the amount of

data, which includes both the initial spin-up phase and nighttime intervals previously shown to be less accurately represented. Consequently, model performance during daytime conditions is likely better than these overall metrics suggest.

It is also worth noting that Ts1 and Ts2, both foliage temperature measurements, show noticeable differences. This can be attributed vegetation species heterogeneity or uneven plant health. These factors add bias to the validation and should be taken into account when interpreting the results.

The air temperature results indicate a strong similarity between the meteorological data from the Météo-France station (used as boundary conditions in the simulation), the experimental measurements taken above the green roof, and the outputs of the Solene-microclimat model. This agreement is expected, given that the large-scale air temperature, which is relatively homogeneous, was directly imposed as a boundary condition in the model.

However, the validation was performed at the building scale. Results indicate that the Solene-microclimat model satisfactorily reproduces green roof temperatures at this scale. However, in the subsequent analysis, the model will be applied at the urban block scale.

3.2. Sensitivity analysis

Temperatures were computed for July 27, 2018, from 7 AM to 9 PM. The results are depicted for 4 PM as it represents the daily temperature peak where differences are most important. Additionally, 8 PM results are shown to capture evening effects.

How each parameter influences the outcomes of green roofs is examined, specifically focusing on air temperature 2 meters above the roof, pedestrian air temperature, humidity and heat index.

For each tetrahedron of the mesh of the urban morphologies, temperatures from low and high scenarios simulations are compared to the base scenario. The differences (Tair(scenario) - Tair(base scenario) for example) are shown using violin plots with the median marked by a black dot. A positive difference indicates a cooling effect compared to base scenario. These plots represent all mesh elements without loss of information.

3.2.1. Green roof air temperature

Fig 6 depicts the comparison of the 12 parameters to the base scenario for air temperature 2m above the green roof and Tab 3 presents the parameter influence on green roof air temperature, averaged across all archetypes.

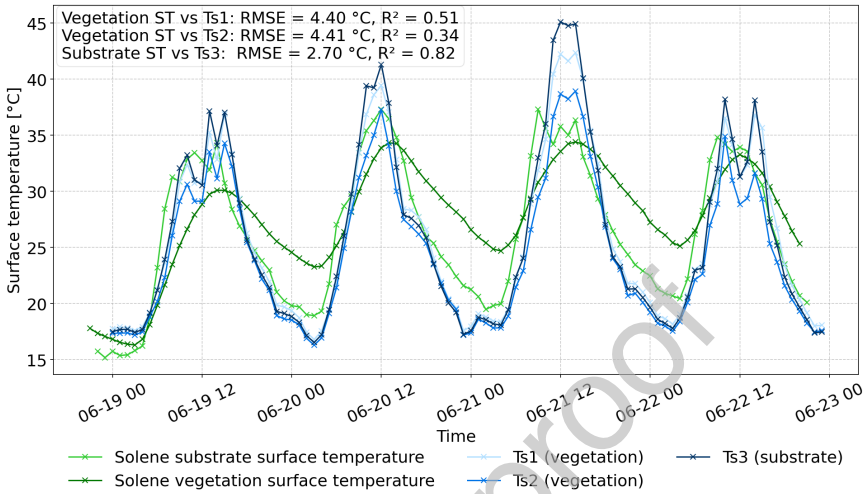

(a) Surface temperatures. The statistical indicators are computed model and measurements, for vegetation and substrate surface temperatures and for the whole period.

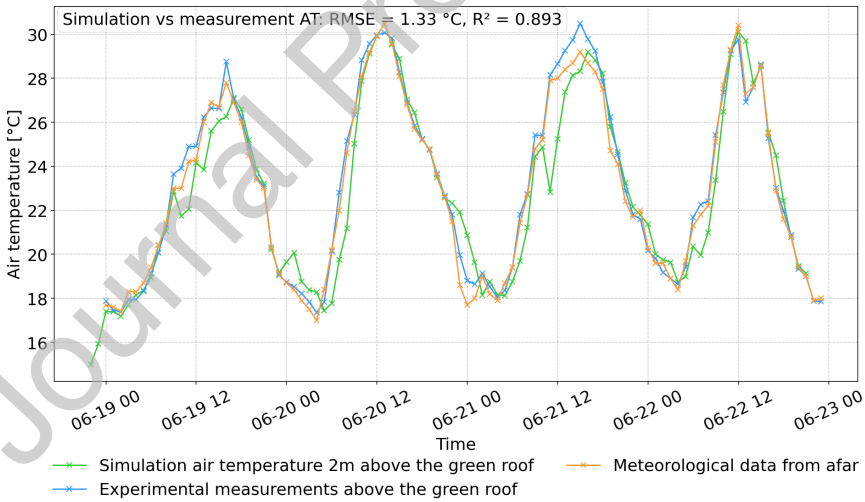

(b) Air temperatures. The statistical indicators are computed from simulation air temperature 2m above the green roof and experimental measurements above the green roof and for the whole period.

Figure 5: Validation results : Solene and measurements temperatures.

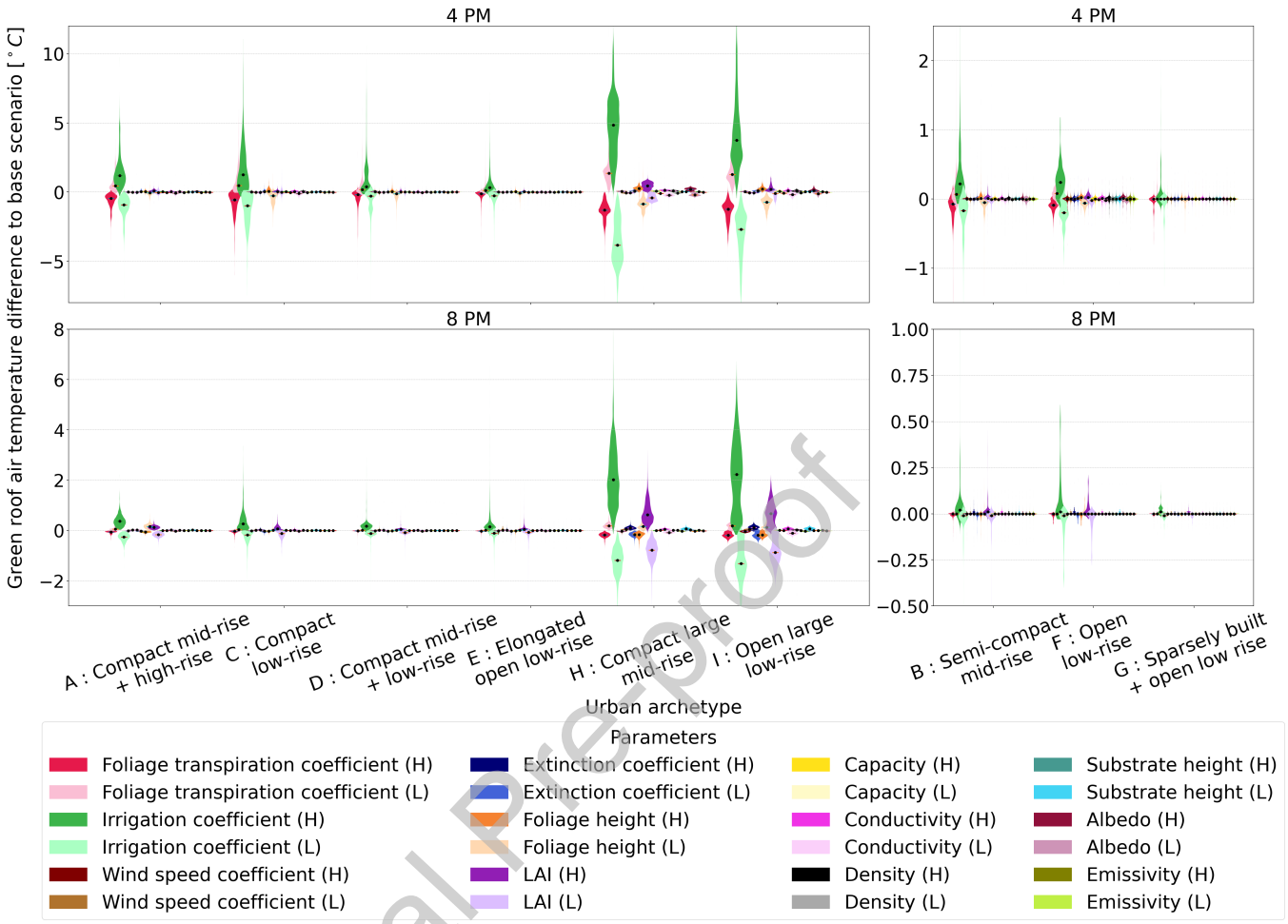

Figure 6: Above green roof air temperature reduction (compared to base scenario) for 4 PM (top) and 8 PM (bottom). H = high and L = low specify the parameter value that was modified compared to base scenario.

Across all urban block archetypes and at both 4 PM and 8 PM, the irrigation coefficient stands out as the most influential parameter affecting green roof air temperature (1.4 and 0.5°C influence on average for low and high values at 4PM and 8PM). This is consistent with the fact that evapotranspiration is the primary cooling mechanism on green roofs [70]. Since the irrigation coefficient reflects the vegetation's moisture availability, it directly controls evapotranspiration rates and thus significantly impacts air temperature. A high irrigation coefficient promotes greater evaporative cooling by diverting more solar energy towards water evaporation rather than heat storage. The foliage transpiration coefficient, which determines the partitioning of evapotranspiration between plant transpiration and soil evaporation, is the second influential parameter at 4 PM (0.6°C influence). At 4 PM, foliage height emerges as the third most influential parameter (0.15°C influence). Notably, decreasing foliage height below the base level significantly warms

	Average parameter influence on green roof air temperature [°C]			
Parameter	**Low - 4 PM**	**High - 4 PM**	**Low - 8 PM**	**High - 8 PM**
Foliage transpiration coefficient	0.573	-0.564	0.063	-0.063
Irrigation coefficient	-1.207	1.623	-0.396	0.647
Wind speed coefficient	-0.024	0.018	0.019	-0.017
Extinction coefficient	0.037	-0.023	-0.053	0.033
Foliage height	-0.300	0.091	0.070	-0.055
LAI	-0.076	0.109	-0.254	0.204
Capacity	-0.036	0.023	0.000	0.004
Conductivity	-0.085	0.043	-0.034	0.021
Density	-0.027	0.032	-0.001	0.007
Substrate height	0.012	0.013	0.022	-0.008
Albedo	-0.049	0.047	-0.002	0.002
Emissivity	-0.007	0.005	-0.003	0.003

Table 3: Parameter influence on green roof air temperature, averaged across all archetypes. A positive sign means the parameter change raises air temperature 2-m above the green roof.

the air, whereas increasing it above the base provides only limited additional cooling. At 8 PM, LAI has more influence than foliage height (0.2 to 0.05 $°C$ influence). Although the influence of parameters is similar across the block archetypes, the irrigation coefficient, LAI, foliage transpiration and foliage height have a higher impact for compact large mid-rise and open large low-rise archetypes compared to other archetypes.

Table 4 presents how the green roof air temperature varies with the 12 parameters and the physical explanations beneath these impacts. The influence of the parameters on air temperature arises from opposing effects on the foliage and substrate layers due to their distinct thermal and physical characteristics. For instance, increasing the extinction coefficient and LAI reduces the transmission of solar radiation through the foliage, thereby increasing absorption in the canopy while limiting energy reaching the substrate. However, because foliage has a low heat capacity and a large surface area (with high LAI) exposed to air, it heats up quickly but also cools efficiently via convection. The substrate, on the other hand, has a higher thermal mass and limited exposure, so it warms more slowly but retains heat longer. This can result in prolonged heating of the canopy air layer when the LAI and extinction coefficient are low.

Similarly, a higher foliage transpiration coefficient increases the proportion of evapotranspiration that comes from plant transpiration rather than soil evaporation. This leads to a cooler foliage surface temperature, but potentially a warmer substrate surface, as less water is available for evaporative cooling from the substrate. As with the extinction coefficient and LAI, this highlights the importance of concentrating energy exchange processes in the foliage, which can more efficiently regulate heat.

Finally, increasing foliage height and wind speed coefficient enhances convective exchanges between

the canopy air and the ambient atmosphere. During the day, this promotes the upward transfer of heat from the canopy to the atmosphere, contributing to a cooling effect. At night, when the ambient air is generally cooler, stronger convection accelerates the cooling of the canopy air. However, the net effect depends on the temperature gradient and the time of night: in the early evening, mixing may initially raise the green roof air temperature by blending warmer canopy air with cooler ambient air. This is evident in the 8 PM results, where an increase in foliage height is actually associated with a rise in air temperature. As the night progresses, this same mixing promotes faster cooling, potentially resulting in lower temperatures later in the night.

It is important to note that all results related to substrate properties are highly sensitive to the simulation setup, particularly the short (half a day) simulation period and the assumption of a fixed indoor air temperature, which together constrain the extent to which substrate heat dynamics can fully develop.

Table 4: Impact of parameters on green roof air temperature. A positive sign means an increase in the parameter raises air temperature 2-m above the green roof.

Parameter	**4 PM**	**8 PM**	**Impact of increasing the parameter**
Foliage transpiration coefficient	+	+	Larger plant transpiration cools foliage but reduces substrate evaporation; overall, canopy air temperature tends to rise.
Irrigation coefficient	-	-	Promotes greater evapotranspiration, reducing heat in foliage and substrate, leading to cooler green roof air.
Wind speed coefficient	-	-	Increased convection with ambient air causes cooling.
Extinction coefficient	+	+	More solar radiation absorbed by foliage reduces substrate radiation but increases substrate heating, raising air temperature.
Foliage height	-	+	Higher foliage increases convection cooling but also thermal inertia, delaying evening cooling.
LAI	-	-	Denser foliage reduces solar transmission and substrate heating, enhancing convective cooling.
Substrate height, capacity and density	-	-	Greater substrate thermal inertia slows heating, reducing heat transfer to canopy air and cooling the roof.
Conductivity	-	-	Improved heat transfer between cool indoor and outdoor layers lowers green roof temperature.
Albedo	-	-	Higher reflectivity reduces heat gain, especially during daytime.
Emissivity	-	-	Enhanced longwave emission cools surface, especially at night.

3.2.2. Air temperature and humidity rate at pedestrian level

Pedestrian air temperature and relative humidity are computed for each parameter variation and compared to the base scenario. Results are shown at 4 PM and 8 PM across the nine urban block archetypes (Fig. 7 and 8).

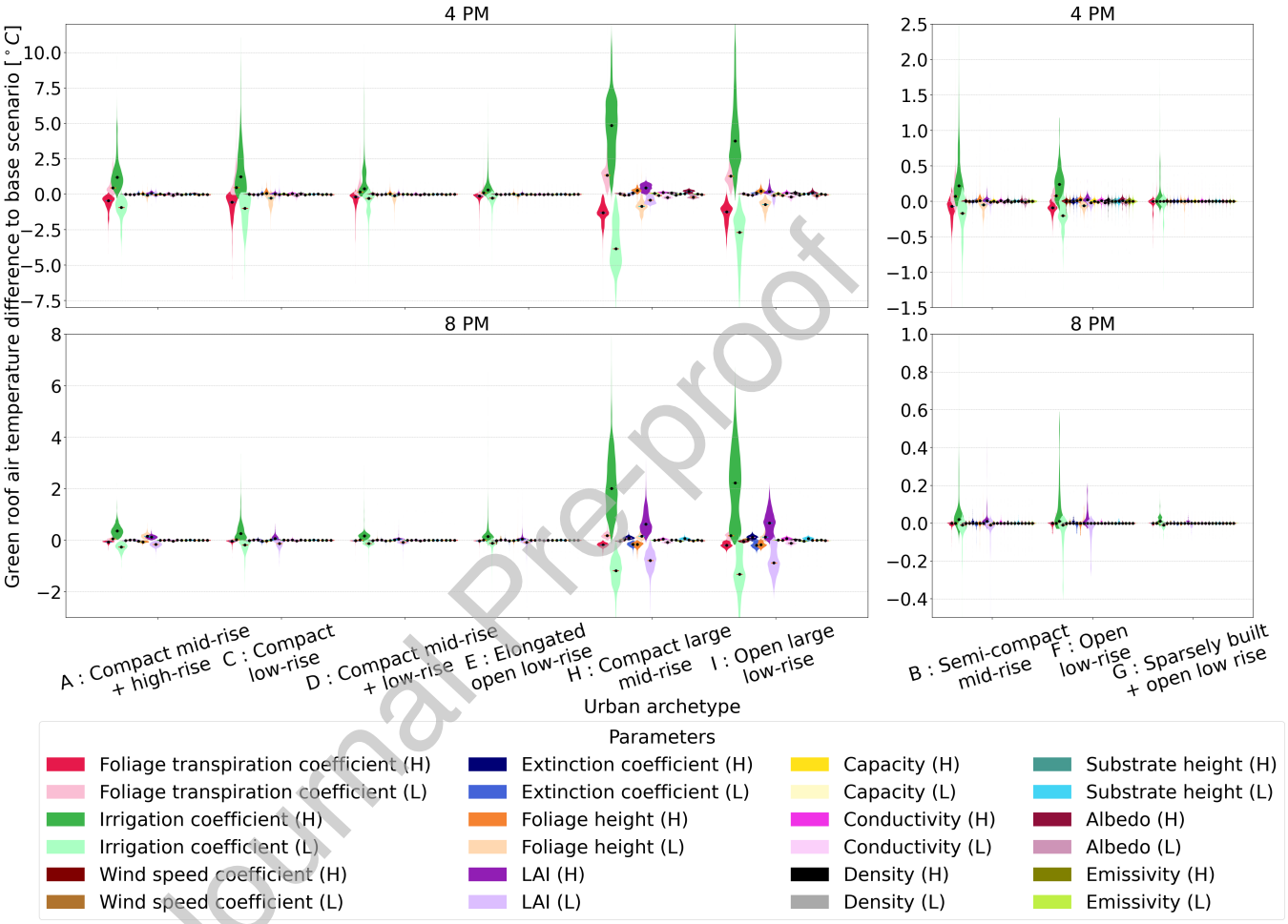

Figure 7: Pedestrian air temperature reduction (compared to base scenario) for 4 PM (top) and 8 PM (bottom). H = high and L = low specify the parameter value that was modified compared to base scenario.

Regarding pedestrian air temperature, the influence of each parameter mirrors that observed on green roof air temperature, which is expected given that the impact of green roof on pedestrian air temperature is majorly driven by convective exchanges with the air above the green roof.

Variations in mean relative humidity can reach up to 2 %, and their patterns differ from those observed for temperature. Since higher humidity tends to reduce comfort in warm conditions, some configurations that lower air temperature may actually lower comfort. For example, increasing the irrigation coefficient

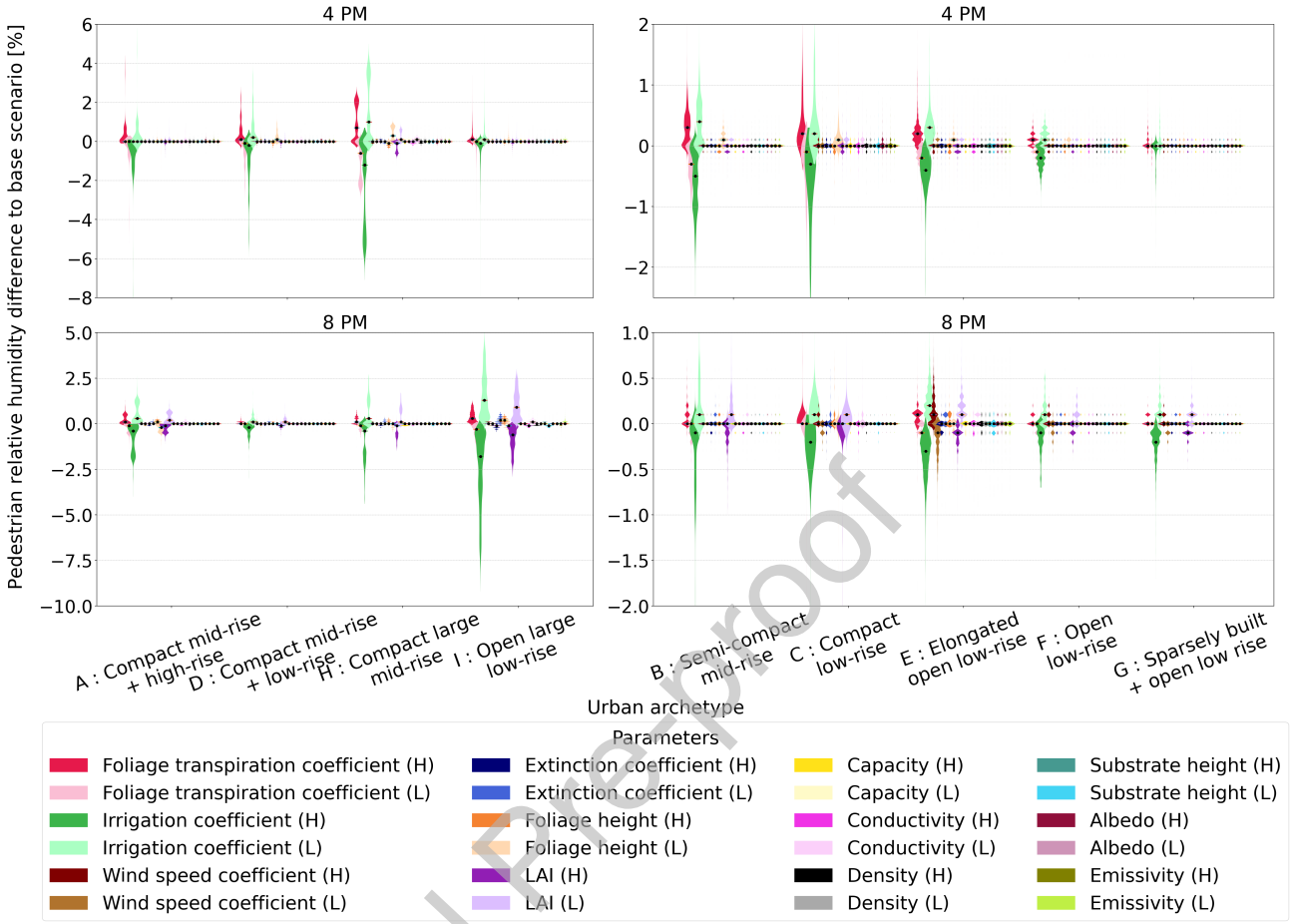

Figure 8: Pedestrian relative humidity reduction (compared to base scenario) for 4 PM (top) and 8 PM (bottom). H = high and L = low specify the parameter value that was modified compared to base scenario.

or LAI leads to lower pedestrian air temperatures but simultaneously results in higher humidity levels. This relationship is explained further in the next section with heat index.

3.2.3. Pedestrian heat index

Figure 9 shows the heat index, integrating the combined influence of pedestrian air temperature and relative humidity on perceived thermal comfort. The heat index results mimic the results of pedestrian air temperature. The similarity between the heat index graph (Fig. 9) and the pedestrian air temperature graph (Fig. 7) indicates that green roof parameters have a stronger influence on air temperature than on humidity, relative to their respective contributions to the heat index. Therefore when combining air temperature and humidity in the heat index, the parameters' influence are of the same sign as for the air temperature.

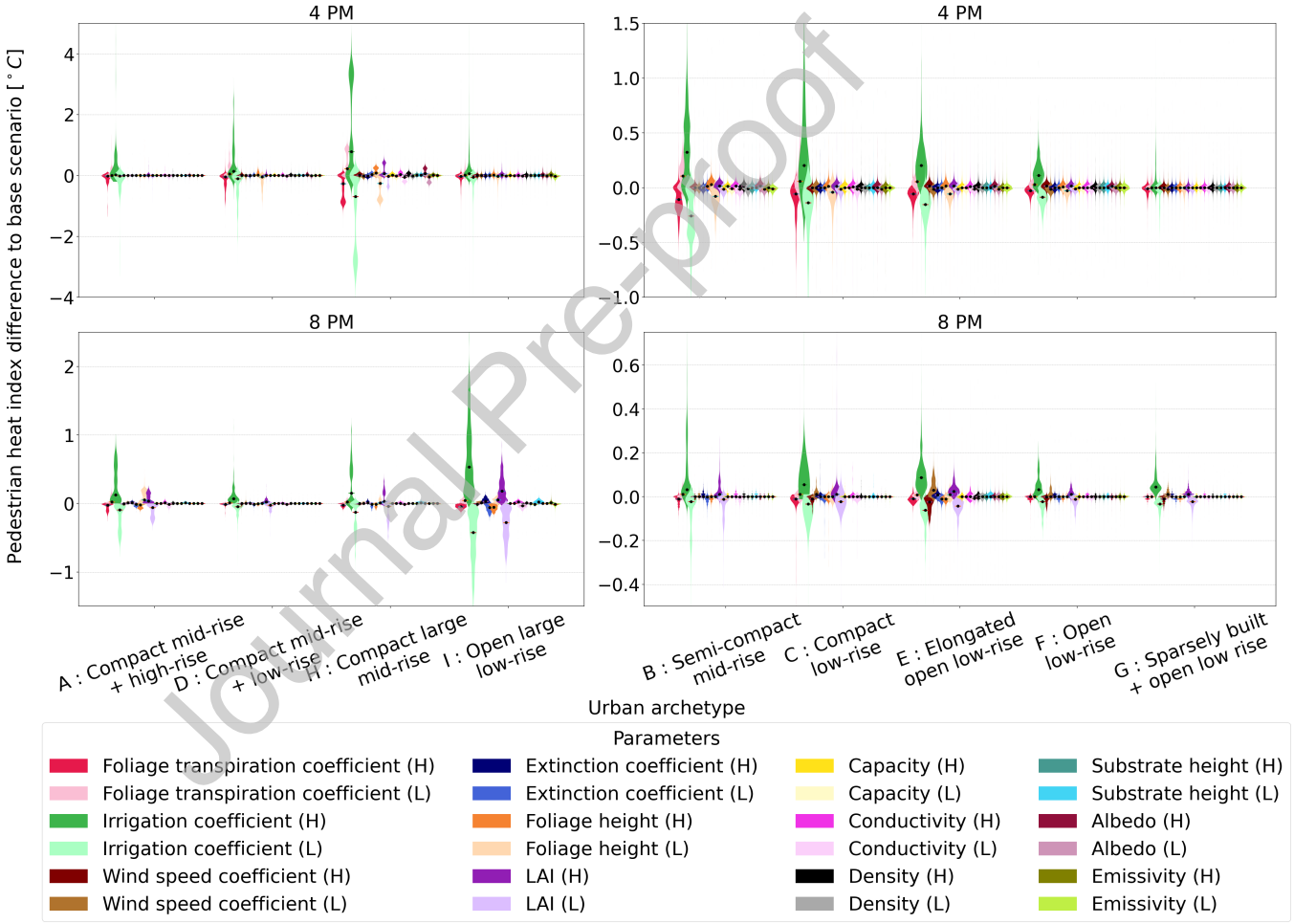

Figure 9: Pedestrian heat index reduction (compared to base scenario) for 4 PM (top) and 8 PM (bottom). H = high and L = low specify the parameter value that was modified compared to base scenario.

Overall, the heat index values range between 36 °C and 40 °C. According to the official classification by the U.S. National Weather Service, this falls within the 'Extreme Caution' category (32 – 41 °C), where pro-

longed exposure or physical activity could lead to heat-related illness. Even if these values are indicative, this highlights the importance of reducing the heat index, even by a fraction of a degree.

4. Discussion

4.1. Green roof parameters : influential & uncertain

Although there are noticeable differences in parameter impact across different hours, the top four most influential parameters remain consistent throughout the day. While the evapotranspiration coefficient appears to have a significantly greater influence on pedestrian temperature, it also comes with higher uncertainty compared to other parameters (see a larger variation range in Table 2). Here, a parameter's uncertainty is defined as the range of values it can take. The wider this range, the more possible values researchers must choose from, which increases uncertainty in simulations when parameters haven't been experimentally determined.

To address this issue of varying uncertainty, the influence of each parameter on pedestrian heat index is scaled by the range of its variation. This provides an estimate of the influence per unit change in the parameter, under the assumption of a linear relationship between parameter variation and pedestrian temperature response. A practical way to reveal each parameter's relative influence is to compute the average heat index difference it causes across archetypes, then divide the result by the range between its low, default, and high values. This ratio offers a more comparable metric of influence across parameters. This process is called scaling. Parameters were then ranked according to this scaled (S) influence on pedestrian heat index.

Table 5 summarizes the parameters rankings at 4 PM and 8 PM, based on both impact and uncertainty. For the influence ranking, both scaled (divided by the range of values of the parameter) and the non-scaled (straight influence on pedestrian heat index) are depicted. The uncertainty ranking is determined by calculating the percentage increase from the base value to the high value, and similarly, the percentage decrease to the low value. The six most uncertain parameters are marked with a U, and the six most influential (based on cumulative rank across both times) are marked with an I.

This scaling helps explain why parameters such as emissivity may appear to have little impact: their input ranges are small due to high certainty, not because they are inherently unimportant. At 8 PM convection takes a more important place than at 4 PM, therefore wind speed coefficient and extinction coefficient have more impact. While at 4 PM, solar radiation dominates, making albedo more influential.

Influential parameters are those for which small variations lead to significant changes in the heat index, while uncertain parameters are those with a wide possible range of values. The most critical parameters in this context are those that are both influential and uncertain. The irrigation coefficient, foliage height, and LAI fall into this category.

Parameter	Low-Default-High	Uncertainty ranking	Impact ranking at 4 PM (S)	Impact ranking at 8 PM (S)	Type
Foliage transpiration coefficient [–]	0.5 - 0.75 - 1	7	2 (2)	3 (4)	x - I
Irrigation coefficient [–]	0.1 - 0.75 - 1.5	1	1 (1)	1 (1)	U - I
Wind speed coefficient [–]	0.8 - 1 - 1.2	11	7 (5)	3 (3)	x - I
Extinction coefficient [–]	0.5 - 0.7 - 0.9	9	11 (11)	6 (5)	x- x
Foliage height [m]	0.05 - 0.25 - 0.5	2	3 (4)	4 (7)	U - I
LAI [-]	1 - 2.5 - 5	3	5 (7)	2 (2)	U - I
Substrate heat capacity $[J.kg^{-1}.K^{-1}]$	700 - 950 - 1200	10	9 (9)	11 (11)	x - x
Substrate conductivity $[W.m^{-1}.K^{-1}]$	0.2 - 0.6 - 1	4	6 (8)	7 (8)	U - x
Substrate density $[kg.m^{-3}]$	600 - 950 - 1300	6	8 (10)	10 (10)	U - x
Substrate thickness [m]	0.1 - 0.2 - 0.3	5	12 (12)	8 (9)	U - x
Foliage albedo [-]	0.2 - 0.3 - 0.4	7	4 (6)	12 (12)	x - x
Foliage emissivity [-]	0.85 - 0.9 - 0.95	12	10 (3)	9 (6)	x - I

Table 5: More uncertain parameters: U stands for uncertain, I for influential. Impact rankings with scaled values are given in parentheses.

Table 6 presents the average reduction in pedestrian heat index associated with selected parameters, compared to base scenario. Only impacts greater than ± 0.1°C (for average of all walkable surfaces) are shown, as this threshold was chosen to represent a meaningful effect (as decided in [71]). Among all tested parameters, only four exceed this threshold in several urban block archetypes: foliage transpiration coefficient, irrigation coefficient, foliage height, and LAI. The parameter influence on pedestrian air temperature, averaged across all archetypes, for all parameters is provided in Appendix, with Table 14.

The results show that to effectively reduce urban overheating through green roofs, irrigation is essential. Transitioning from a medium-moisture to a well-irrigated green roof improves pedestrian temperature by an average of 0.4°C across all urban archetypes, reaching up to 1.4°C for the compact large mid-rise archetype.

Another key benefit of irrigation is plant survival. Without sufficient water, vegetation may die, greatly reducing the effectiveness of green roofs. This study assumes healthy, living vegetation and does not capture the diminished benefits of dead or poorly maintained green roofs.

Regarding vegetation characteristics, the effects of LAI and foliage height were assessed independently, making it difficult to precisely quantify their combined impact. However, increasing both density and height from medium to high is expected to slightly improve pedestrian comfort.

Parameters	A	B	C	D	E	F	G	H	
Foliage transpiration coefficient (high)	-0.11	-0.11	x	-0.23	x	x	x	-0.37	
Foliage transpiration coefficient (low)	x	0.11	x	0.23	x	x	x	0.35	
Irrigation factor (high)	0.31 (0.26)	0.36 (0.11)	0.28	0.69 (0.21)	0.24	0.14	0.19	1.38 (0.28)	0.27 (0
Irrigation factor (low)	-0.22 (-0.19)	-0.27	-0.19	-0.51 (-0.15)	-0.19	-0.10	-0.14	-1.20 (-0.21)	-0.22 (-0
Foliage height (high)	x	x	x	x	x	x	x	0.11	
Foliage height (low)	x	x	x	x	x	x	x	-0.35	
LAI (high)	x	x	x	x	x	x	x	0.16	x (0
LAI (low)	x (-0.10)	x	x	x	x	x	x	-0.12 (-0.13)	x (-0

Table 6: Average impact on heat index at pedestrian level [$^{\circ}C$]: temperature difference relative to the baseline scenario, per urban archetype. In parenthesis values for 8 PM that respect the threshold. Values with an absolute magnitude below 0.1 are marked with a cross. Parameters for which all values were below this threshold are omitted from the table.

In summary, tall, dense, irrigated green roofs offer the most effective cooling solutions. This may also require deeper substrates to support such vegetation, as taller plants often need more growing medium.

The strong influence of irrigation parameters, LAI, and foliage height observed in this study as well as the overall influence of improving the green roof parameters are consistent with findings reported in the literature. First, as shown by the majority of sensitivity analysis studies summarized in Table 1, LAI and soil thickness are generally identified as the most influential parameters affecting green roof cooling performance; however, irrigation-related factors were not explicitly investigated in these studies.

Second, Wang et al. (2022) [72] compared two city-scale scenarios in Berlin (Cfb climate) assuming 100 %green roof implementation, with and without irrigation, using the WRF model. Averaged over urban grid cells, irrigated green roofs reduced air temperature by 0.71 ˚C, compared to 0.55 $^{\circ}C$ for non-irrigated roofs. In the present study, there is an average temperature difference of 0.427 $^{\circ}C$ (Table 14) between scenarios with moderately moist substrates and well-irrigated green roofs at 4 PM, which is of comparable magnitude.

Third, Morakinyo et al. (2017) [6] investigated green roofs under various climates, urban densities, roof coverage ratios, and configurations (extensive versus intensive) using ENVI-met and EnergyPlus. Their results indicate that green roofs with increased substrate depth and vegetation height achieved approximately twice the cooling effectiveness. Joshi et al. (2024) [25] reported an average cooling effect of about

0.5 °C when comparing green roof scenarios with non-green roof cases with Solene-microclimat, while in the present study the cumulative improvement of green roof parameters at 4 PM reaches approximately 0.7 °C (Table 14). Although the present study does not identify a strong individual influence of vegetation height or substrate depth, the observed doubling of cooling intensity resulting from overall green roof parameter improvements remains consistent with these findings.

Finally, in a Dfa climate, Berardi et al. (2016) [9] showed that increasing LAI enhances daytime air temperature cooling at the pedestrian level by up to 0.4 $^{\circ}C$. Similarly, in this study, increasing LAI led to a maximum air-temperature reduction of 0.38 $^{\circ}C$ for archetype H (Table 6), although the average effect across archetypes remained below 0.1 ˚C (Table 14.

4.2. Variation across urban archetypes

The aim here is to understand how the urban morphology of the archetypes explains the varying influence of green roof parameters on the different metrics used. Fig. 10 displays key characteristics of the urban archetypes, helping to interpret the variations in results observed between them.

Archetypes H and I show the strongest parameter influences on green roof air temperature, both in terms of average effect and variability (see Fig. 7). The results are similar to what Joshi et al. (2024) observed. These archetypes also feature the largest green roof areas, both in total surface and in the size of individual roofs. Although archetype A has a similar percentage of green roof coverage as archetype I, the parameter impacts differ significantly. This could be explained by the fact that archetype A consists of smaller green roofs located at varying altitudes, leading to weaker interactions between green roofs, potentially accounting for the observed differences. To explore this further, the analysis uses a proximity-weighted green roof density metric (PWGRD) that quantifies the local concentration of green roofs surrounding each green roof mesh element.

It is calculated by summing the surface areas of nearby green roofs, each weighted by the inverse of the square of its distance to the target mesh part, giving more influence to closer surfaces (see Eq. 2).

$$PWGRD_j = \sum_{i=1}^{N} \frac{A_i}{d_{ij}^2} \tag{2}$$

with $PWGRD_j$ the proximity-weighted green roof density metric of the green roof mesh j, A_i the surface area of green roof i, $d_i j$ = the distance from green roof i to the target mesh part j, N the number of green roof surfaces within the considered proximity (150 m radius). This radius is considered based on the results of the cooling distance obtained in the literature. The cooling distance is the length between the center of

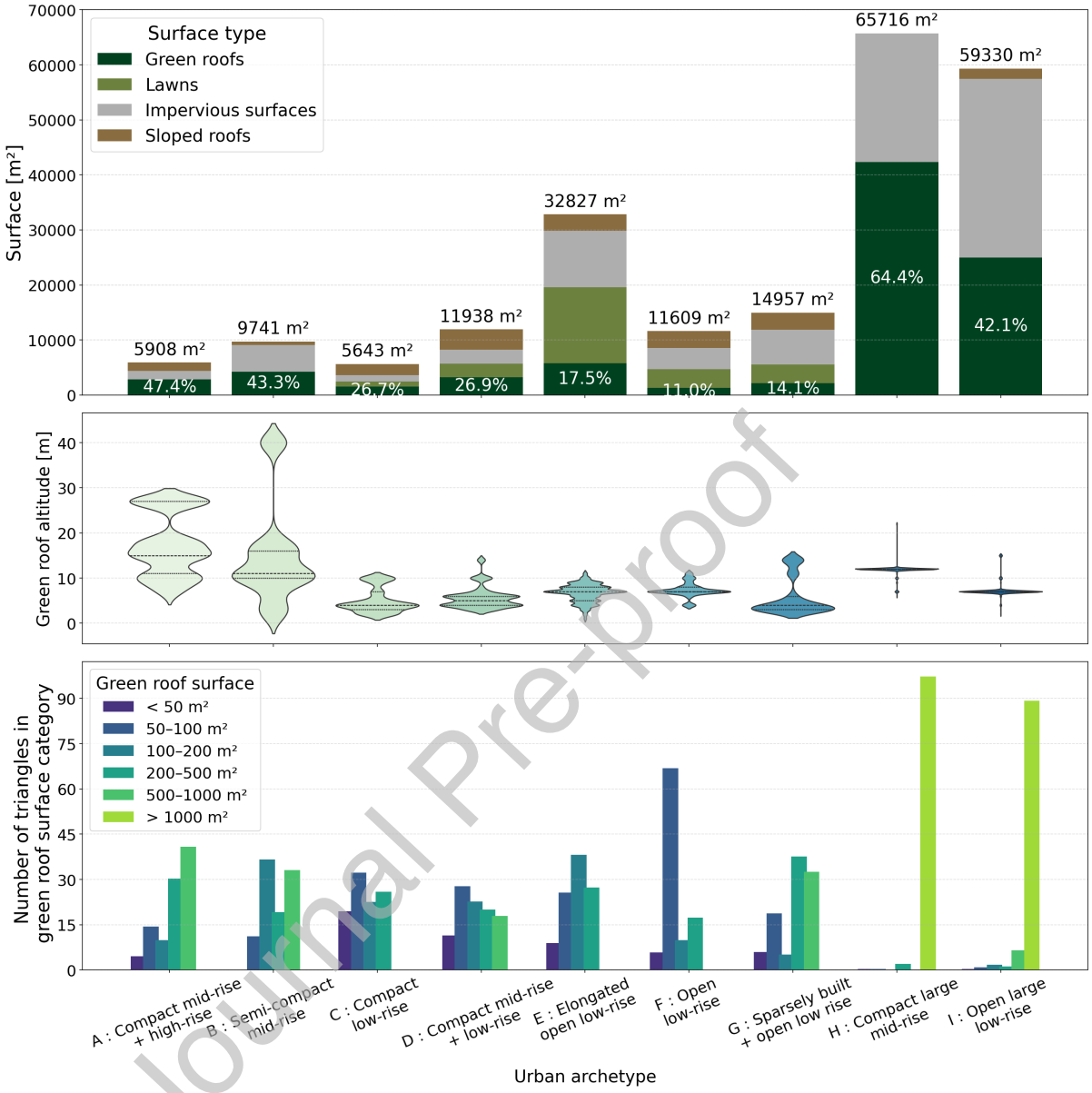

Figure 10: Urban archetypes characteristics

the green roof and the boundary of the cooling area. Soltanifard et al. (2025) [73] reviewed the cooling effect of urban green infrastructure and found that the cooling distance is between 120 and 300 m.

This approach captures not just the quantity but the spatial clustering of green roofs. A radius of 150 meters is used to define the neighborhood around each mesh part, ensuring relevant local interactions are considered. The resulting values are then averaged at the block level, providing an indicator of green roof density per urban archetype. These block-level densities are compared to the high irrigation coefficient

results, computed as the difference from the baseline scenario. To assess the strength of this relationship, a Pearson correlation analysis was conducted. As shown in Fig. 11, the results reveal a strong correlation, suggesting that the spatial distribution of green roofs largely explains the variation in the impact of the irrigation coefficient on green roof air temperature. Indeed, more than 90% of the variance in irrigation coefficient impact is explained by the variance in the green roof proximity-weighted green roof density. The irrigation coefficient was selected for this analysis as it exhibits the most significant variation and is discussed in detail.

Overall, these findings suggest that green roof air temperature is sensitive to parameter changes, especially when green roofs are spatially concentrated. It is important to note that in this analysis, all green roofs share the same parameter values. As a result, nearby green roofs, even if located on different buildings, affect each other: modifying a parameter such as the irrigation coefficient simultaneously for several adjacent roofs amplifies the temperature response. However, in real-world conditions, green roofs on separate buildings are likely to be managed independently. For example, if one building irrigates its green roof while a neighboring one does not, the mutual influence is reduced. This emphasizes once again that a single, large green roof tends to be more effective than multiple smaller, disconnected ones.

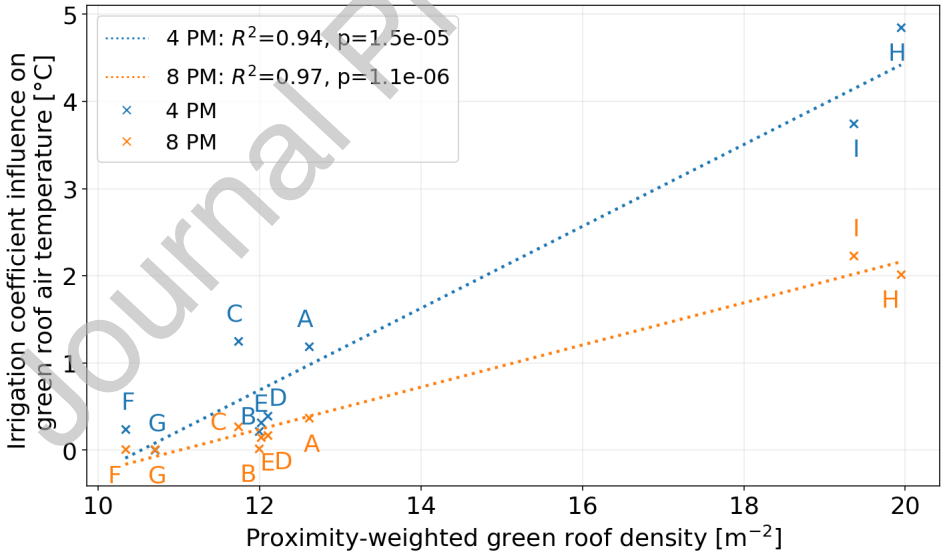

Figure 11: Irrigation coefficient impact (high to base scenarios) on green roof air temperature depending on the proximity weighted green roof density

4.3. Pedestrian values

Some of the differences in parameter impacts on green roof air temperature also help explain their influence at the pedestrian level. In particular, blocks such as F and G, which showed limited sensitivity to green roof parameters at roof level, also exhibit relatively low impacts on pedestrian air temperature and heat index. Archetypes like H and I, which displayed strong parameter influence on green roof temperature, maintain similarly high impacts at the pedestrian level. Previously, how green roof density influences the sensitivity of green roof air temperature to green roof parameters was shown. The next step is to assess how effectively each urban archetype transmits these rooftop temperature changes down to the pedestrian level.

Using the same approach as for the proximity-weighted green roof density, the ground-level green roof density, which quantifies the localized concentration of green roofs around each walkable triangle, is computed. This indicator reflects the density of green roofs as perceived from pedestrian areas. Figure 12 shows the relationship between this ground-level density and the impact of the irrigation coefficient on the heat index at 4 PM. No significant correlation is observed at 8 PM. At 4 PM, however, 63% of the variance in the irrigation coefficient impact on the heat index is explained by the ground-level green roof density. Although this is a weaker correlation than at the roof level, it remains meaningful given that at the pedestrian level, all the characteristics of the archetypes are considered.

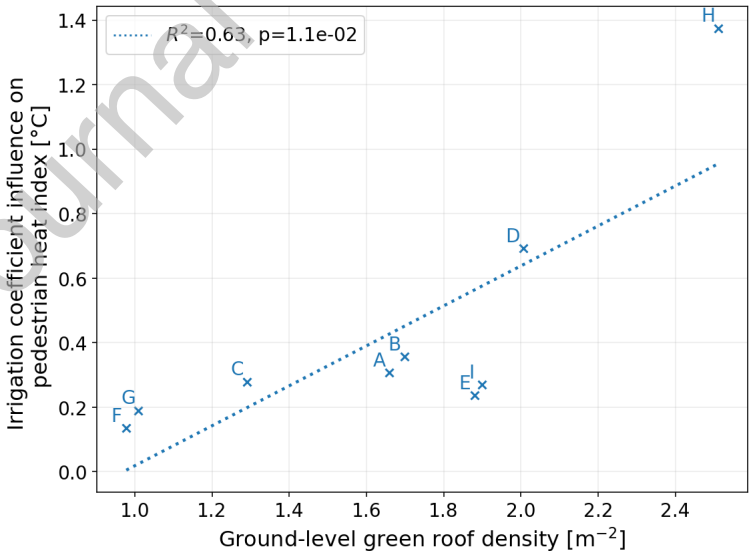

Figure 12: Irrigation coefficient impact (high-base) on the heat index depending on the ground-level green roof density

It is worth noting that H and I display similarly high proximity-weighted green roof densities, indicating

tightly clustered green roof triangles with strong mutual influence. However, H exhibits a much higher ground-level green roof density than I. This difference stems from the layout of walkable paths: in H, pedestrian areas are well distributed around the building and its green roofs, while in I, many walkable areas are located farther away. This spatial arrangement likely explains why, at 4 PM, parameter impacts on the heat index are considerably stronger for H than for I.

Similarly, A, C, and D had comparable impacts on green roof air temperature. However, D had a much greater impact at the pedestrian level, due to its higher ground-level green roof density. In both A and I, a significant portion of the green roof area is located at one corner of the urban block, which limits its influence at 4 PM to nearby zones only. However, later in the evening, air mixing through convection becomes more effective, allowing the cooling effect of the green roof to spread more widely across the block. This behavior is illustrated in Table 6, where A and I are the only two archetypes for which the average reduction in heat index at the pedestrian level at 8 PM is equal to or greater than that observed at 4 PM. For all other archetypes, the cooling impact is more pronounced at 4 PM than at 8 PM. Therefore, both A and I archetypes exhibit an enhanced evening cooling effect.

This result aligns well with the existing literature. Previous studies have shown that temperature reductions associated with green roofs tend to increase with a higher roof-to-ground ratio and lower building heights [72, 6, 74, 75, 76, 25]. As the magnitude of temperature reduction grows, it is reasonable to expect that enhancements in green roof parameters will have an amplified effect. Specifically, when green roofs exert a stronger influence on near-ground air temperatures, any factor affecting roof-level thermal performance is more likely to propagate downward, impacting ground-level conditions as well. Furthermore, While the results cannot be directly generalized due to the specific urban archetypes of Liège, the observed relationship between the irrigation-related coefficient and both ground-level and proximity-weighted green roof density may be applicable to other urban contexts, as these metrics can be computed for any archetype.

Some urban archetypes demonstrate greater effectiveness in cooling the pedestrian level than others. However, these configurations often require extensive green roof coverage, which entails significant renovation efforts and associated costs. To account for both the cooling benefit and the implementation effort, a Thermal Mitigation Ratio (TMR), defined as in Eq 4.3, is introduced:

$$\mathrm{TMR} = \frac{A_{\mathrm{walkable}}}{A_{\mathrm{green\_roof}}} \times I_{\mathrm{IF}} \tag{3}$$

with A_{walkable} the surface area of walkable paths (the area to be cooled), $A_{\mathrm{green\_roof}}$ the surface area of

green roof (the area with investment) and I_{IF} the irrigation coefficient influence on heat index at 4 PM. This ratio is calculated using the irrigation coefficient influence on the heat index at 4 PM. It highlights which urban archetypes benefit most from improvements in green roof parameters, by quantifying their impact on thermal mitigation relative to the effort required to implement green roofs. This metric is computed assuming the implementation effort and the heat index reduction scale linearly with rooftop surface area, which is a simplification. Table 7 presents the results, with archetypes ranked by their thermal mitigation ratio.

Archetype	D	E	G	F	H	B	C	I	A
Thermal mitigation ratio [°C.m^2/m^2]	1.1	1.0	0.9	0.8	0.8	0.4	0.4	0.3	0.2

Table 7: Thermal mitigation ratio per archetype

Joshi et al. [25] ranked urban archetypes by their average ground air temperature under identical meteorological conditions, without green roofs. Their results show that average temperatures can differ by up to 5°C between archetypes. The ranking from highest to lowest air temperature was: H, B, I, A, G, D, C, F, E. These differences were primarily attributed to higher levels of impervious surfaces, greater building density, and increased building heights.

Interestingly, the ranking of archetypes by thermal mitigation ratio (Tab. 7) appears almost reversed. This suggests that the hottest archetypes, with higher levels of impervious surfaces, greater building density, and increased building heights, tend to benefit less from improving parameters. In contrast, less dense and less built-up configurations seem to be more responsive to green roof improvements, making them more favorable candidates for such strategies.

For archetypes D and E, for example, enhancing a green roof from medium moisture to well irrigated conditions on a 1 m^2 area results in an approximate reduction of 1 °C in heat index for 1 m^2 of walkable area at pedestrian level. As previously discussed, this mitigation effect arises from complex physical interactions at the block scale and cannot be directly extrapolated to other urban configurations or to scaled-down versions of these blocks.

However, the effort to green the roofs and maintain them is not the same for all archetypes and buildings. First, in certain configurations, the feasibility of installing green roofs is influenced by building ownership. For example, it is generally easier to implement green roofs on archetypes H and I, which represent commercial centers, than on archetype D, which consists primarily of individual houses. Nevertheless, some archetypes are more prevalent in Liège. In particular, archetype D is the most common [49]. Second, green roofs are usually feasible on flat roofs [77]. However, supporting intensive green roofs

(dense, irrigated, with thicker substrates) add considerable weight on the buildings. Whether the buildings can support such green roofs depends on the reserved structural capacity of the buildings, which needs further investigation before implementation.

4.4. Influence of meteorological conditions on the green roof parameter sensitivity

It has been found that in hot–humid regions, the evaporative cooling potential of vegetation is reduced compared to hot–dry regions. Furthermore, the cooling effect of green roofs is lower under conditions of low solar radiation and high relative humidity [78, 11], both on specific days and, by extension, in regions characterized by such conditions. For instance, Morakinyo et al. [6] investigated the performance of green roofs across different climates using ENVI-met and EnergyPlus. Their results indicate that overall daytime cooling effectiveness follows this order: hot–dry, hot–humid, warm–humid, and temperate.

It should be noted that these results are based on simulations with fixed irrigation settings that are independent of local climate. Thus, they do not account for water stress in arid regions, where irrigation may be limited, nor for water availability in non-irrigated green roofs, which may be less critical in humid regions.

As a result, the sensitivity of model parameters may vary. Under more humid conditions, the influence of the irrigation coefficient may be reduced. Under higher solar radiation, parameters governing the absorption and interception of solar fluxes, such as albedo or LAI, may become more influential. Under windier conditions, sensitivity to wind speed–related parameters may decrease. A comprehensive assessment of these interactions could be achieved in future work through a global sensitivity analysis that jointly considers meteorological variables and green roof parameters.

5. Conclusion

Solene-microclimat results were compared to measurements in very hot summer meteorological conditions. Findings are that the model reproduces the physical processes of green roofs correctly.

The parameters used for green roof modeling in Solene-microclimat were identified, along with their plausible ranges of values. These ranges were established based on a literature review, providing useful reference values when no specific data are available. For each parameter, a baseline, high, and low value were selected to assess their individual influence on several outputs: air temperature above the green roof, pedestrian level air temperature and humidity, and the resulting heat index. This analysis was conducted across nine urban archetypes representative of the city of Liège, Belgium with realistic greening. It enables a detailed examination of how green roof properties interact with urban morphology to affect pedestrian thermal comfort.

For the parameters considered, changes that decrease air temperature at pedestrian level often result in higher relative humidity, which may in turn reduce thermal comfort. However, when combining both factors using the heat index, the cooling effect generally remains significant, although it is partially offset by the rise in humidity. Irrigation proves essential for maximizing the cooling potential of green roofs; well-irrigated systems can reduce pedestrian level temperatures by up to 1.4 $°C$ compared to medium irrigated ones. Tall and dense vegetation further enhances cooling performance. Increasing both density and height from medium to high is expected to improve pedestrian comfort by at least $0.1°C$. Modeling green roofs requires numerous parameters, each subject to varying levels of uncertainty. These parameters were classified based on their influence on cooling performance and their associated uncertainty.

Four parameters emerge as both highly influential and relatively uncertain: the two irrigation related parameters, foliage density (LAI), and foliage height. This study shows that other parameters, such as those related to substrate properties, have little to no effect on pedestrian thermal comfort. However, simulations were performed over a short period of time, and substrate parameters may become more relevant over longer simulations, with inertia effects. Overall, relative parameter rankings and trends are more reliable than absolute temperature or heat index values, as they are likely less sensitive to meteorological conditions and model parameterization.

Regarding the archetypes, the effect of green roof parameters on roof air temperature depends strongly on how green roof surfaces are spatially distributed. When green roofs are large and closely grouped, parameter adjustments yield a greater cooling impact. The influence of green roofs on the heat index along walkable paths is closely linked to the proximity of green roofs to these paths. The nearer the green roofs

are to these pedestrian areas, the stronger their effect on thermal comfort. To account for both cooling effectiveness and implementation effort, a thermal mitigation ratio was introduced, ranking archetypes based on the amount of walkable area cooled per unit of green roof implemented. This metric highlights that while some configurations achieve good thermal outcomes, they often require disproportionately large green roof areas to cool relatively small pedestrian zones. The compact mid-rise + low-rise archetype was found to have the best thermal mitigation ratio.

However, several limitations of this study should be acknowledged. First, parameter sensitivity is context-dependent. The observed impacts of each parameter are influenced by the values assigned to the others. The current approach does not allow conclusions on the combined effects of interdependent variables, such as LAI and foliage height, or the two irrigation parameters. A global sensitivity analysis involving the most influential parameters is necessary to better understand their interactions. Given the computational demands, such analyses could be focused on a limited number of configurations.

Furthermore, nighttime cooling was not assessed. This study focused on daytime conditions for a single extreme heat day, with some results in early evening. Yet, nighttime thermal discomfort plays a critical role in urban heat stress, especially during heat waves. The effects of green roofs on nocturnal cooling should be explored in future research.

In addition, heat index was used as the sole metric for thermal comfort. While this indicator captures combined effects of temperature and humidity, it does not account for radiant heat exchange and wind effects. Including mean radiant temperature would provide a more comprehensive evaluation of pedestrian thermal comfort. Although the Solene-microclimat tool allows such calculations, their high computational cost prevented their inclusion in this study. Future work could incorporate this dimension.

Finally, the results depend on several hypotheses. Meteorological conditions, for instance, significantly influence green roof performance. High relative humidity has been shown to suppress evapotranspiration and reduce latent heat flux. As such, the outcomes presented here are highly sensitive to the weather conditions. Future studies could explore how irrigation strategies affect cooling potential under more humid conditions. Additionally, indoor temperature was fixed, limiting the representation of building thermal dynamics. This assumption limits the analysis to buildings with cooling systems and might reduce the observable influence of substrate properties on cooling performance. Furthermore, the simulations covered only half a day and therefore did not capture how buildings store and release heat over longer periods. Extending the analysis to multiple days would provide a better understanding of the long-term cooling potential of green roofs. Lastly, a local sensitivity analysis was performed, which allowed the

identification of influential parameters but did not capture potential interaction effects between them. A global sensitivity analysis, applied to all parameters or to the four most influential ones, would be necessary to further investigate these combined effects.

Declaration of interests

The authors declare that they have no known competing financial interests or personal relationships that could have appeared to influence the work reported in this paper.

Acknowledgments

This research used computational resources of the Snellius supercomputer provided by SURFsara and funded by the Netherlands Organization for Scientific Research (NWO). Computational resources have also been provided by the Consortium des Équipements de Calcul Intensif (CÉCI), funded by the Fonds de la Recherche Scientifique de Belgique (F.R.S.-FNRS) under Grant No. 2.5020.11 and by the Walloon Region. We gratefully acknowledge the support and access to these facilities.

Appendix A

5.1. Sensitivity analysis modeling additional information

Type of surface	Material	Height [m]	Albedo [-]	Emissivity [-]
Walls	Concrete	0.3	0.3	0.9
Impervious surfaces	Asphalt Concrete	0.1 1	0.2	0.9
Lawns	Foliage Soil	0.05 0.15	0.25	0.9
Roofs	Concrete	0.2	0.3	0.9

Table 8: Surfaces composition for the local sensitivity analysis

Type of material	Conductivity [$W.m^{-1}.K^{-1}$]	Specific heat [$J.kg^{-1}.K^{-1}$]	Density [$kg.m^{-3}$]
Asphalte	0.75	950	2100
Concrete	1.75	1000	2300
Soil	0.70	900	1600

Table 9: Thermophysical properties of materials used

Type of building	Composition
Wall	30 cm concrete
Roof	20 cm concrete
Green roof	10 cm substrate, 5 cm drainage layer, 15.5 cm concrete, 10 cm false ceiling
Street	10 cm asphalt, 1 m concrete

Table 10: Composition of walls and roofs

Material	Conductivity [$W.m^{-1}.K^{-1}$]	Specific heat [$J.kg^{-1}.K^{-1}$]	Density [$kg.m^{-3}$]
Concrete	1.75	1000	2300
Drainage layer	0.1	600	500
False ceiling	0.21	840	900
Asphalt	0.75	950	2100

Table 11: Material description for the experimental validation

631 *5.2. Experimental validation modeling additional information*

632 *5.3. Process-related parameters derivation*

633 The model incorporates adjustment coefficients that distinguish soil evaporation and plant transpiration
634 and account for both plant characteristics and water stress to calculate a more suitable evapotranspiration
635 (ET) (Eq. 4).

$$ET = (K_s K_{cb} + K_e) \times ET_0 \tag{4}$$

636 Solene-microclimat introduces two key parameters: the irrigation coefficient (f), and the foliage tran-
637 spiration coefficient (α_{lat}). These parameters are directly used in the evapotranspiration calculation to
638 approximate vegetation response under varying moisture conditions, according to Eq. 5.

$$\begin{aligned} \phi_{lat,f} &= \alpha_{lat} \times f \times ET_0 \\ \phi_{lat,se} &= (1 - \alpha_{lat}) \times f \times ET_0 \end{aligned} \tag{5}$$

639 with :

640 • $\phi_{lat,f}$ the latent heat flux from the foliage (crop transpiration)

641 • $\phi_{lat,se}$ the latent heat flux from the ground surface (soil evaporation)

642 • α_{lat} that quantifies the part of transpiration in evapotranspiration

643 • f that quantifies the magnitude of evapotranspiration

644 • K_s the water stress coefficient

645 • K_{cb} the basal crop coefficient

- K_e the soil evaporation coefficient

To approximate the crop coefficient K_{cb}, tabulated values corresponding to vegetation types typically found on green roofs are consulted. Common examples include turf grass ($K_{cb,ref} = 0.8$), mint ($K_{cb,ref} = 1.1$), and alfalfa ($K_{cb,ref} = 1.15$). For the purposes of this study, a representative value of $K_{cb} = 1$ is adopted.

Several formulations of soil moisture extractions functions (K_s) exist in the literature (e.g., [79]), many of which express the ratio of actual to potential evapotranspiration as a function of the current soil water content relative to field capacity. This study adopts the commonly used and simplest formulation given by $K_s = \frac{\theta}{\theta_{FC}}$ [80], where θ is the current volumetric water content and θ_{FC} is the water content at field capacity.

For the soil evaporation coefficient, and following the methodology outlined in [57], the expression is derived under the assumption of $K_{cb} = 1$ as in Eq. 6.

$$K_e = min \begin{cases} 0.2 \times \frac{0.5\theta_{WP} - \theta}{0.5\theta_{WP} - \theta_{FC}} \\ 1.2 \times exp(-k_s \times LAI) \end{cases} \tag{6}$$

with θ_{WP} the wilting point and θ_{FC} the field capacity. Finally the two coefficients are expressed as in Eq. 7.

$$\begin{aligned} f &= \frac{\theta}{\theta_{FC}} + K_e \\ \alpha_{lat} &= \frac{\frac{\theta}{\theta_{FC}}}{\frac{\theta}{\theta_{FC}} + K_e} \end{aligned} \tag{7}$$

Assuming the wilting point ranges between 0.03 and 0.15 $m^3\ m^{-3}$, the field capacity between 0.2 and 0.4 $m^3 m^{-3}$, that the water stress coefficient K_s varies between 0 and 1, and taking into account the previously defined variation ranges of the LAI and extinction coefficient, the resulting variation ranges for the irrigation coefficient and the foliage transpiration coefficient are respectively 0 to 1.5 and 0.5 to 1.

5.4. Parameter ranges

Reference	**LAI** [−]	**Foliage height** [m]	**Emissivity** [−]	**Albedo** [−]
[30]	0.15 - 4.95	0.05 - 0.95	0.81 - 0.99	0.15 - 0.45
[39]	0.1 - 5	0.1 - 0.3	x	x
[35]	1 - 6	0.05 - 0.5	x	x
[41]	0.5 - 5	x	x	x
[36]	0.5 - 5	x	1	0.3
[81]	3	0.3	0.9	0.2
[82]	1-5	0.03	0.95	0.22
[83]	2.2	0.035	x	0.29
[84]	2.5	0.2	0.95	0.22
[85]	0.1-5	0.2	x	x
[6]	2	0.3-1	0.95	0.35
[40]	0.1-5	0.3	0.95	0.22
[86]	2.8-5	0.05-0.475	0.97	0.155-0.22
[33]	0.001-3.5[a]-5	0.005-0.3[a]-1	0.8-0.95[a]-1	0.05-0.22[a]-0.5
[32]	0.001-2.5[a]-5	0.01-0.5[a]-1	0.8-0.9[a]-1	0.1-0.25[a]-0.4
[42]	0.1-1[b]-5	0.01-0.1[b]-1	0.8-0.95[b]-1	0.05-0.22[b]-0.5
Values selected	1-2.5-5	0.05-0.25-0.5	0.85-0.9-0.95	0.2-0.3-0.4

Table 12: Vegetation parameters in parametric green roof studies and low, medium and high values chosen for this study. [a] Some studies assume normally distributed parameters; reported here as min–mean–max. [b] Values reported as min–default–max.

Reference	**Thickness** $[m]$	**Conductivity** $[W.m^{-1}.K^{-1}]$	**Density** $[kg.m^{-3}]$	**Specific heat** $[J.kg^{-1}.K^{-1}]$
[42]	0.15	0.2-0.7[b]-1.5	300-500 [b]-2000	300-1000[b] - 2000
[81]	0.1	0.4	x	x
[82]	0.08	0.4	641	1000
[83]	0.2	0.25	1600	890
[84]	0.1	0.35	1100	1200
[87]	0.15-0.75	0.2	1020	1093
[85]	0.1	0.35	1100	1200
[6]	0.3	0.9	1850	850
[40]	0.15	0.85	1639	1800
	0.15	0.28	730	1100
[33]	0.05-0.25[a]-0.7	0.2-0.4[a]-1.5	300-641[a]-2000	500-1000[a]-2000
[41]	0.05 - 0.3	x	x	x
[35]	0.05 - 0.5	x	x	x
[39]	0.15	0.208	1100	730
	0.15	0.85	1800	1639
[36]	0.04 - 0.15	x	x	x
[29]	x	0.15-0.85[a]-4	x	100-720[a]-2000
[30]	0.06 - 0.66	0.250 - 1.45	400 - 1990	520 - 1990
[65][c]	x	0.2	873.2	788
	x	0.21	759.6	923
	x	0.284	772.7	1360
	x	0.288	748.4	546
	x	0.229	724	375
Values selected	0.1-0.2-0.3	0.2-0.6-1	600-950-1300	700-950-1200

Table 13: Substrate parameters ranges used in parametric green roof studies, and low, medium and high values chosen for this study. [a] Some studies assume normally distributed parameters; reported here as min–mean–max.[b] Values reported as min–default–max. [c] Based on experimental substrate characterization.

	Average parameter influence on pedestrian heat index [°C]			
Parameter	**Low - 4 PM**	**High - 4 PM**	**Low - 8 PM**	**High - 8 PM**
Foliage transpiration coefficient	0.121	-0.127	0.020	-0.021
Irrigation coefficient	-0.336	0.427	-0.152	0.206
Wind speed coefficient	-0.014	0.011	0.015	-0.014
Extinction coefficient	0.009	-0.007	-0.020	0.012
Foliage height	-0.106	0.030	0.022	-0.019
LAI	-0.028	0.033	-0.092	0.063
Capacity	-0.012	0.008	-0.001	0.002
Conductivity	-0.029	0.015	-0.015	0.009
Density	-0.010	0.010	-0.001	0.003
Substrate height	0.003	0.004	0.008	-0.002
Albedo	-0.024	0.023	0.000	0.000
Emissivity	-0.009	0.004	-0.003	0.002

Table 14: Parameter influence on pedestrian heat index, averaged across all archetypes. A positive sign means the parameter change raises air temperature 2-m above the green roof.

References

[1] T. R. Oke, G. Mills, A. Christen, J. A. Voogt, Urban Climates, Cambridge University Press, 2017. https://doi.org/10.1017/9781139016476.

[2] M. Santamouris, Regulating the damaged thermostat of the cities—status, impacts and mitigation challenges, Energy and Buildings 91 (2015) 43–56. https://doi.org/10.1016/j.enbuild.2015.01.027.

[3] B.-J. He, J. Wang, H. Liu, G. Ulpiani, Localized synergies between heat waves and urban heat islands: Implications on human thermal comfort and urban heat management, Environmental Research 193 (2021) 110584. https://doi.org/10.1016/j.envres.2020.110584.

[4] C. P. Skelhorn, G. Levermore, S. J. Lindley, Impacts on cooling energy consumption due to the uhi and vegetation changes in manchester, UK, Energy and Buildings 122 (2016) 150–159. https://doi.org/10.1016/j.enbuild.2016.01.035.

[5] Z. Liu, W. Cheng, C. Jim, T. E. Morakinyo, Y. Shi, E. Ng, Heat mitigation benefits of urban green and blue infrastructures: A systematic review of modeling techniques, validation and scenario simulation in ENVI-met v4, Building and Environment 200 (2021) 107939. https://doi.org/10.1016/j.buildenv.2021.107939.

[6] T. E. Morakinyo, K. Dahanayake, E. Ng, C. L. Chow, Temperature and cooling demand reduction by green-roof types in different climates and urban densities: A co-simulation parametric study, Energy and Buildings 145 (2017) 226–237. https://doi.org/10.1016/j.enbuild.2017.03.066.

[7] M. Detommaso, A. Gagliano, L. Marletta, F. Nocera, Sustainable urban greening and cooling strategies for thermal comfort at pedestrian level, Sustainability 13 (6) (2021). https://doi.org/10.3390/su13063138.

[8] H. Akbari, S. Konopacki, Energy effects of heat-island reduction strategies in Toronto, Canada, Energy 29 (2) (2004) 191–210. https://doi.org/10.1016/j.energy.2003.09.004.

[9] U. Berardi, The outdoor microclimate benefits and energy saving resulting from green roofs retrofits, Energy and Buildings 121 (2016) 217–229. https://doi.org/10.1016/j.enbuild.2016.03.021.

[10] M. Santamouris, Cooling the cities – A review of reflective and green roof mitigation technologies to fight heat island and improve comfort in urban environments, Solar Energy 103 (2014) 682–703. https://doi.org/10.1016/j.solener.2012.07.003.

[11] E. Jamei, H. W. Chau, M. Seyedmahmoudian, A. Stojcevski, Review on the cooling potential of green roofs in different climates, Science of The Total Environment 791 (2021) 148407. https://doi.org/10.1016/j.scitotenv.2021.148407.

[12] P. Bevilacqua, The effectiveness of green roofs in reducing building energy consumptions across different climates. a summary of literature results, Renewable and Sustainable Energy Reviews 151 (2021) 111523. https://doi.org/10.1016/j.rser.2021.111523.

[13] S. Vera, C. Pinto, P. C. Tabares-Velasco, W. Bustamante, A critical review of heat and mass transfer in vegetative roof models used in building energy and urban environment simulation tools, Applied Energy 232 (2018) 752–764. https://doi.org/10.1016/j.apenergy.2018.09.079.

[14] S. Gaffin, et al., Energy balance modeling applied to a comparison of green and white roof cooling efficiency, in: Third Annual International Greening Rooftops for Sustainable Communities, Green Roof for Healthy Cities, Washington, D.C., 2005.

[15] Z.-H. Wang, E. Bou-Zeid, J. A. Smith, A coupled energy transport and hydrological model for urban canopies evaluated using a wireless sensor network, Quarterly Journal of the Royal Meteorological Society 139 (675) (2013) 1643–1657. https://doi.org/10.1002/qj.2032.

[16] C. S. de Munck, A. Lemonsu, R. Bouzouidja, V. Masson, R. Claverie, The GREENROOF module (v7.3) for modelling green roof hydrological and energetic performances within TEB, Geoscientific Model Development 6 (6) (2013) 1941–1960. https://doi.org/10.5194/gmd-6-1941-2013.

[17] E. Alexandri, P. Jones, Temperature decreases in an urban canyon due to green walls and green roofs in diverse climates, Building and Environment 43 (4) (2008) 480–493, part Special: Building Performance Simulation. https://doi.org/10.1016/j.buildenv.2006.10.055.

[18] N. Yaghoobian, J. Srebric, Influence of plant coverage on the total green roof energy balance and building energy consumption, Energy and Buildings 103 (2015) 1–13. https://doi.org/10.1016/j.enbuild.2015.05.052.

[19] S. S. G. Hashemi, H. B. Mahmud, M. A. Ashraf, Performance of green roofs with respect to water quality and reduction of energy consumption in tropics: A review, Renewable and Sustainable Energy Reviews 52 (2015) 669–679. https://doi.org/10.1016/j.rser.2015.07.163.

[20] N. H. Wong, Y. Chen, C. L. Ong, A. Sia, Investigation of thermal benefits of rooftop garden in the tropical environment, Building and Environment 38 (2) (2003) 261–270. https://doi.org/10.1016/S0360-1323(02)00066-5.

[21] M. Musy, M.-H. Azam, S. Guernouti, B. Morille, A. Rodler, The SOLENE-Microclimat Model: Potentiality for Comfort and Energy Studies, 2021, pp. 265–291. https://doi.org/10.1007/978-3-030-65421-4_13.

[22] L. Malys, Évaluation des impacts directs et indirects des façades et des toitures végétales sur le comportement thermique des bâtiments, PhD thesis, Ecole Centrale de Nantes, Nantes, France (2012). http://www.theses.fr/2012ECDN0052.

[23] L. Malys, M. Musy, C. Inard, A hydrothermal model to assess the impact of green walls on urban microclimate and building energy consumption, Building and Environment 73 (2014) 187–197. https://doi.org/10.1016/j.buildenv.2013.12.012.

[24] M. Musy, L. Malys, C. Inard, Assessment of direct and indirect impacts of vegetation on building comfort: A comparative study of lawns, green walls and green roofs, Procedia Environmental Sciences 38 (2017) 603–610, sustainable synergies from Buildings to the Urban Scale. https://doi.org/10.1016/j.proenv.2017.03.134.

[25] M. Y. Joshi, A. Rodler, M. Musy, S. Guernouti, J. Teller, Influence of urban morphology on potential of green roofs in regulating local microclimate: A case study of Liège, Belgium, Urban Climate 58 (2024) 102144. https://doi.org/10.1016/j.uclim.2024.102144.

[26] T. Susca, Green roofs to reduce building energy use? A review on key structural factors of green roofs and their effects on urban climate, Building and Environment 162 (2019) 106273. https://doi.org/10.1016/j.buildenv.2019.106273.

[27] A. Saltelli, K. Chan, E. M. Scott, Sensitivity Analysis in Practice: A Guide to Assessing Scientific Models, John Wiley & Sons, 2004. https://doi.org/10.1002/0470870958.

[28] J. Mao, J. H. Yang, A. Afshari, L. K. Norford, Global sensitivity analysis of an urban microclimate system under uncertainty: Design and case study, Building and Environment 124 (2017) 153–170. https://doi.org/10.1016/j.buildenv.2017.08.011.

[29] J. Yang, Z.-H. Wang, Physical parameterization and sensitivity of urban hydrological models: Application to green roof systems, Building and Environment 75 (2014) 250–263. https://doi.org/10.1016/j.buildenv.2014.02.006.

[30] Y. Zhang, L. Zhang, L. Ma, Q. Meng, P. Ren, Cooling benefits of an extensive green roof and sensitivity analysis of its parameters in subtropical areas, Energies 12 (22) (2019). https://doi.org/10.3390/en12224278.

[31] Z. Liu, K. Y. Cheng, T. Sinsel, H. Simon, C. Jim, T. E. Morakinyo, Y. He, S. Yin, W. Ouyang, Y. Shi, E. Ng, Modeling microclimatic effects of trees and green roofs/façades in ENVI-met: Sensitivity tests and proposed model library, Building and Environment 244 (2023) 110759. https://doi.org/10.1016/j.buildenv.2023.110759.

[32] G. Peri, G. Rizzo, G. Scaccianoce, M. La Gennusa, P. Jones, Vegetation and soil – related parameters for computing solar radiation exchanges within green roofs: Are the available values adequate for an easy modeling of their thermal behavior?, Energy and Buildings 129 (2016) 535–548. https://doi.org/10.1016/j.enbuild.2016.08.018.

[33] M. M. Liu, Probabilistic prediction of green roof energy performance under parameter uncertainty, Energy 77 (2014) 667–674. https://doi.org/10.1016/j.energy.2014.09.043.

[34] S. Tsang, C. Jim, Theoretical evaluation of thermal and energy performance of tropical green roofs, Energy 36 (5) (2011) 3590–3598. https://doi.org/10.1016/j.energy.2011.03.072.

[35] T. G. Theodosiou, Summer period analysis of the performance of a planted roof as a passive cooling technique, Energy and Buildings 35 (9) (2003) 909–917. https://doi.org/10.1016/S0378-7788(03)00023-9.

[36] Y. He, H. Yu, A. Ozaki, N. Dong, S. Zheng, Influence of plant and soil layer on energy balance and thermal performance of green roof system, Energy 141 (2017) 1285–1299. https://doi.org/10.1016/j.energy.2017.08.064.

[37] M. Kazemi, R. Rahif, L. Courard, S. Attia, Sensitivity analysis and weather condition effects on hygrothermal performance of green roof models characterized by recycled and artificial materials' properties, Building and Environment 237 (2023) 110327. https://doi.org/10.1016/j.buildenv.2023.110327.

[38] R. Zahedi, S. Daneshgar, O. N. Farahani, A. Aslani, Thermal analysis model of a building equipped with green roof and its energy optimization, Nature-Based Solutions 3 (2023) 100053. https://doi.org/10.1016/j.nbsj.2023.100053.

[39] S. Vera, C. Pinto, F. Victorero, W. Bustamante, C. Bonilla, J. Gironás, V. Rojas, Influence of plant and substrate characteristics of vegetated roofs on a supermarket energy performance located in a semiarid climate, Energy Procedia 78 (2015) 1171–1176, 6th International Building Physics Conference, IBPC 2015. https://doi.org/10.1016/j.egypro.2015.11.089.

[40] S. Vera, C. Pinto, P. C. Tabares-Velasco, W. Bustamante, F. Victorero, J. Gironás, C. A. Bonilla, Influence of vegetation, substrate, and thermal insulation of an extensive vegetated roof on the thermal performance of retail stores in semiarid and marine climates, Energy and Buildings 146 (2017) 312–321. https://doi.org/10.1016/j.enbuild.2017.04.037.

[41] D. J. Sailor, T. B. Elley, M. Gibson, Exploring the building energy impacts of green roof design decisions – a modeling study of buildings in four distinct climates, Journal of Building Physics 35 (4) (2012). https://doi.org/10.1177/1744259111420076.

[42] F. Olivieri, C. Di Perna, M. D'Orazio, L. Olivieri, J. Neila, Experimental measurements and numerical model for the summer performance assessment of extensive green roofs in a mediterranean coastal climate, Energy and Buildings 63 (2013) 1–14. https://doi.org/10.1016/j.enbuild.2013.03.054.

[43] S. Quezada-García, G. Espinosa-Paredes, A. Vázquez-Rodríguez, J.-J. Ambriz-García, A.-M. Escobedo-Izquierdo,

Sensitivity analysis of a green roof, International Journal of Green Energy 13 (3) (2016) 260–266. https://doi.org/10.1080/15435075.2014.952420.

[44] M. Shaterabadi, H. Karimi, H. Mehrjerdi, Advanced modelling of green roof-enabled plus-ZEB energy systems: A synergistic approach using taguchi design and neural networks, Renewable Energy 256 (2026) 124314. https://doi.org/10.1016/j.renene.2025.124314.

[45] N. Balvedi, T. Giglio, Influence of green roof systems on the energy performance of buildings and their surroundings, Journal of Building Engineering 70 (2023) 106430. https://doi.org/10.1016/j.jobe.2023.106430.

[46] M. Robitu, M. Musy, C. Inard, D. Groleau, Modeling the influence of vegetation and water pond on urban microclimate, Solar Energy 80 (2006) 435–447. https://doi.org/10.1016/j.solener.2005.06.015.

[47] T. Robineau, A. Rodler, B. Morille, D. Ramier, J. Sage, M. Musy, V. Graffin, E. Berthier, Coupling hydrological and microclimate models to simulate evapotranspiration from urban green areas and air temperature at the district scale, Urban Climate 44 (2022) 101179. https://doi.org/10.1016/j.uclim.2022.101179.

[48] J. Bouyer, Modélisation et simulation des microclimats urbains - Étude de l'impact de l'aménagement urbain sur les consommations énergétiques des bâtiments, Phd thesis, Université de Nantes, Nantes, France (2009). http://www.theses.fr/2009NANT2035.

[49] M. Y. Joshi, A. Rodler, M. Musy, S. Guernouti, M. Cools, J. Teller, Identifying urban morphological archetypes for microclimate studies using a clustering approach, Building and Environment 224 (2022) 109574. https://doi.org/10.1016/j.buildenv.2022.109574.

[50] L. P. Rothfusz, The heat index "equation" (or, more than you ever wanted to know about heat index), Technical Attachment SR-9023, NWS Southern Region (1990). https://www.weather.gov/media/ffc/ta_htindx.PDF.

[51] H. Fang, F. Baret, S. Plummer, G. Schaepman-Strub, An overview of global leaf area index (LAI): Methods, products, validation, and applications, Reviews of Geophysics 57 (3) (2019) 739–799. https://doi.org/10.1029/2018RG000608.

[52] G. Zheng, L. M. Moskal, Retrieving leaf area index (LAI) using remote sensing: Theories, Methods and Sensors, Sensors 9 (4) (2009) 2719–2745. https://doi.org/10.3390/s90402719.

[53] R. Fieuzal, F. Baup, Estimation of leaf area index and crop height of sunflowers using multi-temporal optical and SAR satellite data, International Journal of Remote Sensing 37 (12) (2016) 2780–2809. https://doi.org/10.1080/01431161.2016.1176276.

[54] S. Luo, C. Wang, F. Pan, X. Xi, G. Li, S. Nie, S. Xia, Estimation of wetland vegetation height and leaf area index using airborne laser scanning data, Ecological Indicators 48 (2015) 550–559. https://doi.org/10.1016/j.ecolind.2014.09.024.

[55] Y. Yuan, X. Wang, F. Yin, J. Zhan, Examination of the quantitative relationship between vegetation canopy height and LAI, Advances in Meteorology 2013 (1) (2013) 964323. https://doi.org/10.1155/2013/964323.

[56] F. Renou-Wilson, C. Barry, C. Mueller, D. Wilson, The impacts of drainage, nutrient status and management practice on the full carbon balance of grasslands on organic soils in a maritime temperate zone, Biogeosciences 11 (08 2014). https://doi.org/10.5194/bgd-11-5557-2014.

[57] Food and Agriculture Organization of the United Nations, Crop evapotranspiration - guidelines for computing crop water requirements, accessed: 2025-02-14 (1998). https://www.fao.org/4/X0490E/x0490e01.htm.

[58] E. P. D. Barrio, Analysis of the green roofs cooling potential in buildings, Energy and Buildings 27 (2) (1998) 179–193. https://doi.org/10.1016/S0378-7788(97)00029-7.

[59] P. C. Tabares-Velasco, J. Srebric, A heat transfer model for assessment of plant based roofing systems in summer conditions, Building and Environment 49 (2012) 310–323. https://doi.org/10.1016/j.buildenv.2011.07.019.

[60] E. Alexandri, P. Jones, Developing a one-dimensional heat and mass transfer algorithm for describing the effect of green roofs on the built environment: Comparison with experimental results, Building and Environment 42 (8) (2007) 2835–2849. https://doi.org/10.1016/j.buildenv.2006.07.004.

[61] W.-M. Wang, Z.-L. Li, H.-B. Su, Comparison of leaf angle distribution functions: Effects on extinction coefficient and fraction of sunlit foliage, Agricultural and Forest Meteorology 143 (1) (2007) 106–122. https://doi.org/10.1016/j.agrformet.2006.12.003.

[62] A. Decruz, Development and integration of a green roof model within whole building energy simulation, Ph.D. thesis, University of Nottingham, Nottingham, UK (2016). https://api.semanticscholar.org/CorpusID:114959025.

[63] P. C. Tabares-Velasco, M. Zhao, N. Peterson, J. Srebric, R. Berghage, Validation of predictive heat and mass transfer green roof model with extensive green roof field data, Ecological Engineering 47 (2012) 165–173. https://doi.org/10.1016/j.ecoleng.2012.06.012.

[64] M. Zhao, P. C. Tabares-Velasco, J. Srebric, S. Komarneni, R. Berghage, Effects of plant and substrate selection on thermal performance of green roofs during the summer, Building and Environment 78 (2014) 199–211. https://doi.org/10.1016/j.buildenv.2014.02.011.

[65] J. Coma, A. de Gracia, M. Chàfer, G. Pérez, L. F. Cabeza, Thermal characterization of different substrates under dried conditions for extensive green roofs, Energy and Buildings 144 (2017) 175–180. https://doi.org/10.1016/j.enbuild.2017.03.031.

[66] T. Keravec-Balbot, A. Rodler, L. Roupioz, M. Musy, T. Gresse, X. Briottet, Identification of urban thermal properties by combining urban microclimate modeling and thermal infrared satellite data, Sustainable Cities and Society 118 (2025) 105995. https://doi.org/10.1016/j.scs.2024.105995.

[67] J. Schwager-Guilloux, Les toitures végétalisées, puits et sources d'éléments en traces métalliques, Ph.D. thesis, 2014LORR0073 (2014). http://www.theses.fr/2014LORR0073.

[68] G. Fraisse, C. Viardot, O. Lafabrie, G. Achard, Development of a simplified and accurate building model based on electrical analogy, Energy and Buildings 15 (2002). https://doi.org/10.1016/S0378-7788(02)00019-1.

[69] L. Malys, M. Musy, C. Inard, Direct and indirect impacts of vegetation on building comfort: A comparative study of lawns, green walls and green roofs, Energies 9 (1) (2016). https://doi.org/10.3390/en9010032.

[70] S. Cascone, J. Coma, A. Gagliano, G. Pérez, The evapotranspiration process in green roofs: A review, Building and Environment 147 (2019) 337–355. https://doi.org/10.1016/j.buildenv.2018.10.024.

[71] M. Žuvela Aloise, R. Koch, S. Buchholz, B. Früh, Modelling the potential of green and blue infrastructure to reduce urban heat load in the city of Vienna, Climatic Change 135 (3-4) (2016) 425–438. https://doi.org/10.1007/s10584-016-1596-2.

[72] X. Wang, H. Li, S. Sodoudi, The effectiveness of cool and green roofs in mitigating urban heat island and improving human thermal comfort, Building and Environment 217 (2022) 109082. https://doi.org/10.1016/j.buildenv.2022.109082.

[73] H. Soltanifard, M. Amani-Beni, The cooling effect of urban green spaces as nature-based solutions for mitigating urban heat: insights from a decade-long systematic review, Climate Risk Management 49 (2025) 100731. https://doi.org/10.1016/j.crm.2025.100731.

[74] H. Chen, R. Ooka, H. Huang, T. Tsuchiya, Study on mitigation measures for outdoor thermal environment on present urban blocks in Tokyo using coupled simulation, Building and Environment 44 (11) (2009) 2290–2299, Special Issue for 2008 International Conference on Building Energy and Environment (COBEE). https://doi.org/10.1016/j.buildenv.2009.03.012.

[75] E. Ng, L. Chen, Y. Wang, C. Yuan, A study on the cooling effects of greening in a high-density city: An experience from Hong Kong, Building and Environment 47 (2012) 256–271, International Workshop on Ventilation, Comfort, and Health in Transport Vehicles. https://doi.org/10.1016/j.buildenv.2011.07.014.

[76] S.-E. Ouldboukhitine, R. Belarbi, D. J. Sailor, Experimental and numerical investigation of urban street canyons to evaluate the impact of green roof inside and outside buildings, Applied Energy 114 (2014) 273–282. https://doi.org/10.1016/j.apenergy.2013.09.073.

[77] M. Y. Joshi, W. Selmi, M. Binard, G.-A. Nys, J. Teller, Potential for urban greening with green roofs: A way towards smart cities, ISPRS Annals of the Photogrammetry, Remote Sensing and Spatial Information Sciences (2020). https://doi.org/10.5194/isprs-annals-VI-4-W2-2020-87-2020.

[78] C. Jim, L. Peng, Weather effect on thermal and energy performance of an extensive tropical green roof, Urban Forestry & Urban Greening 11 (2012) 73–85. https://doi.org/10.1016/j.ufug.2011.10.001.

[79] L. Zhao, J. Xia, C.-y. Xu, Z. Wang, L. Sobkowiak, C. Long, Evapotranspiration estimation methods in hydrological models, Journal of Geographical Sciences 23 (2) (2013). https://doi.org/10.1007/s11442-013-1015-9.

[80] C. Berretta, S. Poë, V. Stovin, Moisture content behaviour in extensive green roofs during dry periods: The influence of vegetation and substrate characteristics, Journal of Hydrology 511 (2014) 374–386. https://doi.org/10.1016/j.jhydrol.2014.01.036.

[81] K. C. Dahanayake, C. L. Chow, Comparing reduction of building cooling load through green roofs and green walls by energyplus simulations, Building Simulation 11 (3) (2018). https://doi.org/10.1007/s12273-017-0415-7.

[82] J.-T. K. Fred Edmond Boafo, J.-H. Kim, Evaluating the impact of green roof evapotranspiration on annual building energy performance, International Journal of Green Energy 14 (5) (2017) 479–489. https://doi.org/10.1080/15435075.2016.1278375.

[83] A. Chan, T. Chow, Energy and economic performance of green roof system under future climatic conditions in Hong Kong, Energy and Buildings 64 (2013) 182–198. https://doi.org/10.1016/j.enbuild.2013.05.015.

[84] S. Yuan, D. Rim, Cooling energy saving associated with exterior greenery systems for three US department of energy (DOE) standard reference buildings, Building Simulation 11 (2018). https://doi.org/10.1007/s12273-018-0427-y.

[85] L. Zhou, Q. Wang, Y. Li, M. Liu, R. Wang, Green roof simulation with a seasonally variable leaf area index, Energy and Buildings 174 (2018) 156–167. https://doi.org/10.1016/j.enbuild.2018.06.020.

[86] M. Vaz Monteiro, T. Blanuša, A. Verhoef, M. Richardson, P. Hadley, R. Cameron, Functional green roofs: Importance of plant choice in maximising summertime environmental cooling and substrate insulation potential, Energy and Buildings 141 (2017) 56–68. https://doi.org/10.1016/j.enbuild.2017.02.011.

[87] I. Ziogou, A. Michopoulos, V. Voulgari, T. Zachariadis, Energy, environmental and economic assessment of electricity savings from the operation of green roofs in urban office buildings of a warm Mediterranean region, Journal of Cleaner Production 168 (2017) 346–356. https://doi.org/10.1016/j.jclepro.2017.08.217.